

Tubuloids derived from human adult kidney and urine for personalized disease modeling

Frans Schutgens^{1,2}, Maarten B Rookmaaker², Thanasis Margaritis³, Anne Rios³, Carola Ammerlaan^{1,2}, Jitske Jansen⁴, Linda Gijzen⁵, Marianne Vormann⁵, Annelotte Vonk⁶, Marco Viveen⁷, Fjodor Yousef Yengej^{1,2}, Sepide Derakhshan³, Karin M. de Winter-de Groot⁸, Benedetta Artegiani¹, Ruben van Boxtel³, Edwin Cuppen⁹, Antoni P. A. Hendrickx⁷, Marry M. van den Heuvel-Eibrink³, Ellen Heitzer¹⁰, Henriette Lanz⁵, Jeffrey Beekman⁶, Jean-Luc Murk^{4,11}, Rosalinde Masereeuw¹⁰, Frank Holstege³, Jarno Drost³, Marianne C Verhaar² and Hans Clevers^{1,3*}

Adult stem cell-derived organoids are three-dimensional epithelial structures that recapitulate fundamental aspects of their organ of origin. We describe conditions for the long-term growth of primary kidney tubular epithelial organoids, or 'tubuloids'. The cultures are established from human and mouse kidney tissue and can be expanded for at least 20 passages (>6 months) while retaining a normal number of chromosomes. In addition, cultures can be established from human urine. Human tubuloids represent proximal as well as distal nephron segments, as evidenced by gene expression, immunofluorescence and tubular functional analyses. We apply tubuloids to model infectious, malignant and hereditary kidney diseases in a personalized fashion. BK virus infection of tubuloids recapitulates in vivo phenomena. Tubuloids are established from Wilms tumors. Kidney tubuloids derived from the urine of a subject with cystic fibrosis allow ex vivo assessment of treatment efficacy. Finally, tubuloids cultured on microfluidic organ-on-a-chip plates adopt a tubular conformation and display active (trans-) epithelial transport function.

Organoid cultures representing different organs can be established from embryonic stem cells or induced pluripotent stem cells (collectively called pluripotent stem cells (PSCs)) and from adult stem cells (ASCs)¹. PSC-derived organoids recapitulate development and have the potential to form structures through processes that only occur during development¹. Typically, PSCs are first expanded and subsequently differentiated toward the fully differentiated (and non-expandable) end product in approximately 2–3 months. PSC-derived organoids have the advantage of structural complexity and are used to study development, hereditary disease and infectious disease (reviewed in refs. ^{1,2}). For tissues that are only formed once and never repaired afterwards, such as the brain, it is the only approach to create organized tissue in vitro. PSC-derived organoids were pioneered for the brain, followed by multiple other organs, including intestine and stomach. PSC-derived 'mini-kidney' organoids have been developed recently that contain cells from all kidney lineages, resulting in strikingly complete 'mini-kidneys'³. However, generation of PSC-derived organoids in a personalized fashion is relatively time-consuming. Primary patient cells (typically fibroblasts) must be reprogrammed into induced PSCs (iPSCs) and subsequently differentiated into the tissue of choice. This procedure takes several months, and the resulting organoids usually cannot be expanded further. The protracted time frame may be especially problematic for personalized cancer drug screening

(by conversion of tumor cells into iPSCs and then back into tumor cells); direct expansion of malignant cells from individual patients in an organoid-type format would be highly preferable.

ASC-derived epithelial organoids recapitulate adult tissue repair rather than development¹. Thus, only tissue compartments that exhibit regenerative capacity are amenable to this approach. ASC-derived organoids are of lower complexity than PSC-derived organoids and to date strictly represent the epithelial parts of organs, with the absence of nerves, blood vessels and stromal elements. The latter may be seen in PSC-derived organoids. These organoids invariably appear as cystic, highly polarized epithelial structures¹. While not representing complete organs to the same extent as PSC-derived organoids, they contain the entire assortment of differentiated, functional epithelial cells and reproduce architectural aspects (such as the spatial distribution of individual cell types) of the original epithelium. ASC-derived organoids can be derived from the pertinent tissues of individuals of any age, typically within 7 d, and do not need to be directed through embryonic development, as they are already fully specified towards the tissue of interest at the start of culture. In contrast to PSC-derived organoids, they can be expanded for many passages while remaining genetically stable¹. As a consequence, they can be cloned at any stage of their culture and are ideally suited for CRISPR-based genomic modification². These characteristics make ASC-organoids a fast and versatile entity for

¹Hubrecht Institute—Royal Netherlands Academy of Arts and Sciences, Utrecht, the Netherlands. ²Department of Nephrology and Hypertension, University Medical Centre Utrecht, Utrecht, the Netherlands. ³Princess Máxima Center for Pediatric Oncology, Utrecht, the Netherlands. ⁴Division of Pharmacology, Utrecht Institute for Pharmaceutical Sciences, Utrecht University, Utrecht, the Netherlands. ⁵Mimetas, Organ-on-a-chip Company, Leiden, the Netherlands. ⁶Regenerative Medicine Center Utrecht, Utrecht, the Netherlands. ⁷Department of Medical Microbiology, University Medical Center Utrecht, Utrecht, the Netherlands. ⁸Wilhelmina Children's Hospital, University Medical Center Utrecht, Utrecht, the Netherlands. ⁹Center for Molecular Medicine, Cancer Genomics Netherlands, Department of Genetics, University Medical Center Utrecht, Utrecht, the Netherlands. ¹⁰Institute of Human Genetics, Medical University of Graz, Graz, Austria. ¹¹Laboratory of Medical Microbiology and Immunology, St. Elisabeth TweeSteden Ziekenhuis, Tilburg, the Netherlands. *e-mail: h.clevers@hubrecht.eu

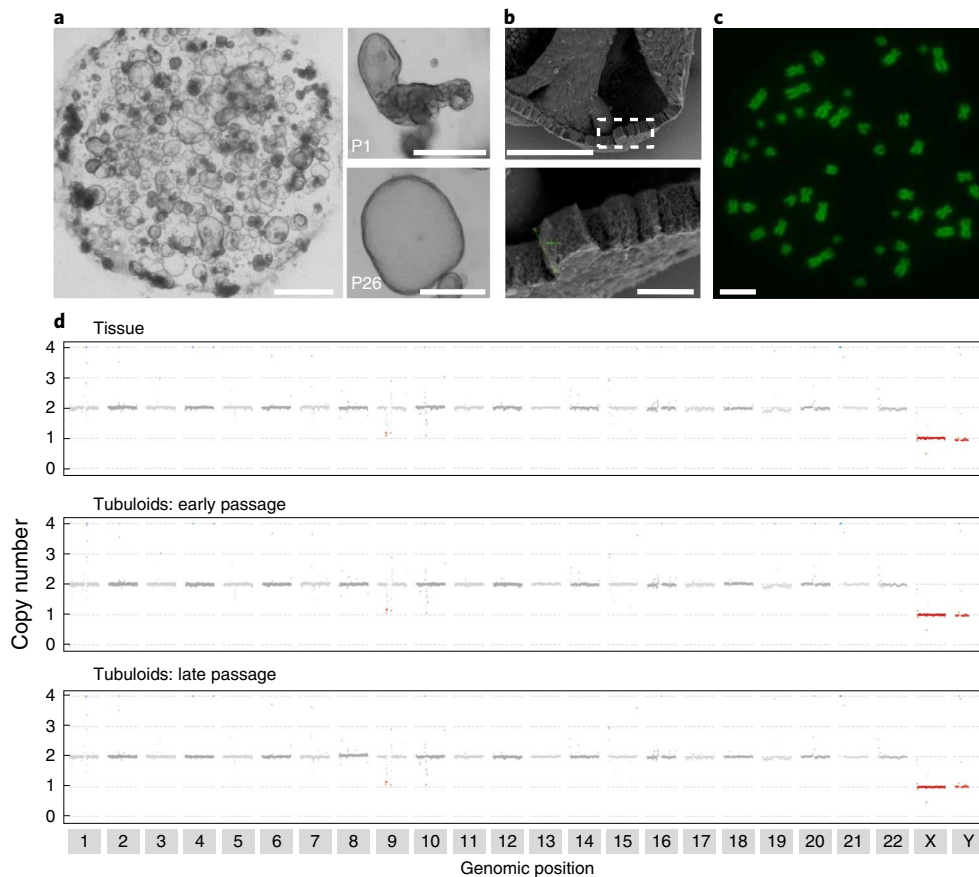


Fig. 1 | Human kidney tubuloid culture. **a**, Tubuloids exhibit a cystic morphology (representative image of >10 independent tubuloid lines). **b**, Scanning electron microscope image of P4 confirms that cystic tubuloids consist of a single layered cuboidal epithelium with cells of approximately 10 μm in diameter (representative image of at least $n=3$ independent tubuloid lines). **c**, An example of a typical normal metaphase spread, from a tubuloid culture after 18 passages (representative image of >40 spreads, from tubuloids in P11, P14 and P18 in 3 independent experiments, from 3 independent tubuloid cultures). **d**, WGS reveals a normal karyogram over short-term (P2) and long-term (P8) cultures (one tubuloid line was used for WGS). Scale bars, 100 μm (**a**, whole droplet); 75 μm (**a**, P1, P26 and **b**); 10 μm (inset of **b** and **c**).

personalized medicine approaches, with the explicit restriction that they only model function and disease of the epithelial elements of their organ of origin.

We originally developed the ASC-organoid technology for the intestine⁴. Similar protocols are now available for many organs and cancers derived thereof (reviewed in refs. ^{1,2}), including liver, prostate, pancreas, stomach, salivary gland, breast, colon and taste buds. These protocols have been applied for cancer modeling and infectious disease modeling, as well as for personalized medicine approaches for cystic fibrosis^{5,6}. Here we extend the approach to the kidney.

Results

Establishing and characterizing kidney tubuloids. To establish a culture protocol sustaining the growth of human kidney tubuloids, we adapted our protocol for the expansion of adult intestinal *Lgr5*⁺ stem cells^{4,7}. We resuspended tubular fragments, obtained after collagenase digestion of cortical human kidney, in Matrigel (Fig. 1a) and added culture media containing (1) R-spondin-conditioned medium to enhance canonical Wnt signaling, known to be essential for kidney homeostasis⁸ and repair⁹; (2) FGF-10, a signal that promotes survival of kidney progenitor cells¹⁰ and that is present in adult kidney¹¹; (3) A8301, to inhibit the TGF- β receptors ALK4/5/7, preventing growth arrest and epithelial to mesenchymal transition¹²; (4) the mitogen epidermal growth factor (EGF); and (5) Rho-kinase inhibitor to prevent anoikis of dissociated cells¹³.

Noggin, Wnt-conditioned medium or Wnt-surrogates¹⁴, nicotinamide and a p38-inhibitor did not increase expansion capacity after 12 weeks of culture and were therefore removed from the medium. Addition of PGE-2 (ref. ¹⁵; after 12 weeks), addition of BMP-4 (for 4 passages) and FGF-2 (in the presence of FGF-10, for 4 passages) did not have a significant effect on expansion capacity.

Kidney tubuloids typically developed within 6 d after seeding (Fig. 1a) as cystic structures consisting of a simple cuboidal epithelium. See Fig. 1b for a scanning electron microscope image of the cells. Under optimized conditions, human tubuloids could be passaged at least 20 times with 1:3 weekly split ratios (Fig. 1a). Tubuloid lines could be established from small tissue samples with 100% efficiency ($n > 30$).

Karyotyping showed that cells retain a normal number of chromosomes over a very long-term culture period (18 passages) (Fig. 1c and Supplementary Fig. 1). Genomic stability was further validated by whole genome sequencing (WGS) analysis of matching early passage (P2) and late passage (P8) tubuloids and of the original kidney tissue. In agreement with karyotyping analysis, we did not observe large chromosomal aberrations by WGS (Fig. 1d). By contrast, chromosomal and/or structural variations occur frequently in embryonic stem cells¹⁶, iPSC¹⁷ and in cell lines such as Madin–Darby canine kidney (MDCK) cells¹⁸. By WGS, we observed 19 mutations in coding regions (of which 15 were missense mutations; Supplementary Fig. 2) in late passage tubuloids compared to

parental tissue and none in the early passage tubuloids. None of these mutations are recurrently found in cancers and none occur in genes that are associated with kidney function or dysfunction. Using a similar protocol, we established long-term mouse tubuloid cultures with essentially 100% efficiency ($n > 10$) that also retained a normal number of chromosomes (Supplementary Fig. 3).

To determine what compartment of the nephron was represented in our system, we performed bulk RNA sequencing (RNA-seq). We compared the transcriptome of cortical kidney tissue samples from three donors with the tubuloid lines established from these. Markers of endothelium (*PECAMI1*, *CDH5*, *FLT1* (ref. 19)) and interstitium/smooth muscle (*MEIS1* (ref. 20), *CALD1* (ref. 21), *PDGFRB* (ref. 22)) were not expressed in tubuloids, whereas (kidney) epithelial (*EPCAM*, *PAX8* (ref. 23)) markers were highly expressed (Fig. 2a). In agreement with the notion that the culture conditions support a regenerative response, we noted increased expression of ASC markers, such as *SOX9* (ref. 24) and *PROM1* (ref. 25). Two stem cell markers of kidney development, *LGR5* (ref. 26) and *SIX2* (ref. 27), were not detected in tissue or in tubuloids. Podocyte markers (*NPHS1*, *WT1*, *PODXL*) were not observed in the tubuloids, whereas proximal tubule markers (*ABCC1*, *ABCC3*, *ABCC4*, *SLC22A3*, *SLC40A1*) were highly expressed. In addition, collecting duct (*CDH1*, *GATA3*, *AQP3*) markers were expressed as well as some markers for loop of Henle (*CLDN10* (ref. 28), *CLDN14* (ref. 29)) and distal tubule (*PCBD1* (ref. 30), *SLC41A3* (ref. 31); Fig. 2a). Thus, the growing structures represent tubular epithelium, exhibit a stem cell signature and lack cell types that are not regenerated in vivo (for example, podocytes³²).

For an in-depth, high-resolution analysis of the epithelial compartment, we performed single-cell RNA-seq. We sorted 192 tubuloid cells and 192 *EPCAM*⁺ epithelial cells (to prevent contamination with blood cells) from the primary cortical kidney tissue from which the tubuloids were derived. After filtering, the median unique transcript number per cell was 13,633. *EPCAM*⁺ kidney epithelial cells and tubuloid cells were assigned to specific cell-cycle phases based on the expression levels of cell cycle-specific genes (Supplementary Fig. 4)³³. As expected, tubuloid cells were fast-cycling. After correction for cell-cycle differences as well as collagenase dissociation-induced stress (a known issue in single-cell RNA-seq experiments on primary tissue³⁴), unsupervised clustering identified seven clusters (Fig. 2b,c). All cells were *PAX8*⁺ and thus kidney epithelial in nature (Supplementary Fig. 5)³⁵. Other epithelial markers were expressed in all clusters, such as *EPCAM*, *KRT18* and *KRT19* (Supplementary Fig. 6). Cluster 1 contained cells derived from primary tissue as well as from tubuloids, characterized by an intercalated cell signature (expression of *SLC4A1*, *SLC26A7*, *ATP6V1B1*) (Supplementary

Fig. 6). Cluster 2 contained the majority of the primary kidney epithelial cells. Clusters 3 to 7 consisted of tubuloid-derived cells. Cluster 4 displayed a collecting duct cell signature (marked by urea-transporter *SLC14A1* (ref. 36) and *CLDN8* (ref. 37)), whereas the signature of cluster 5 implied a proximal tubule cluster (marked by *SLC2A1*, a set of genes involved in glucose handling, and *VEGFA*³⁸). Cluster 7 cells showed increased expression of *COL4A3* and *COL4A4* expression, combined with reduced expression of *KRT18* and *KRT19*, suggestive of an epithelial transition to mesenchymal transition. Clusters 3 and 6 displayed an epithelial signature but did not express segment-specific genes (although cluster 6 showed some expression of the proximal tubule organic cation transporter *SLC22A5* (Supplementary Fig. 6)). The absence of expression of segment-specific genes in clusters 3 and 6 may reflect a progenitor status.

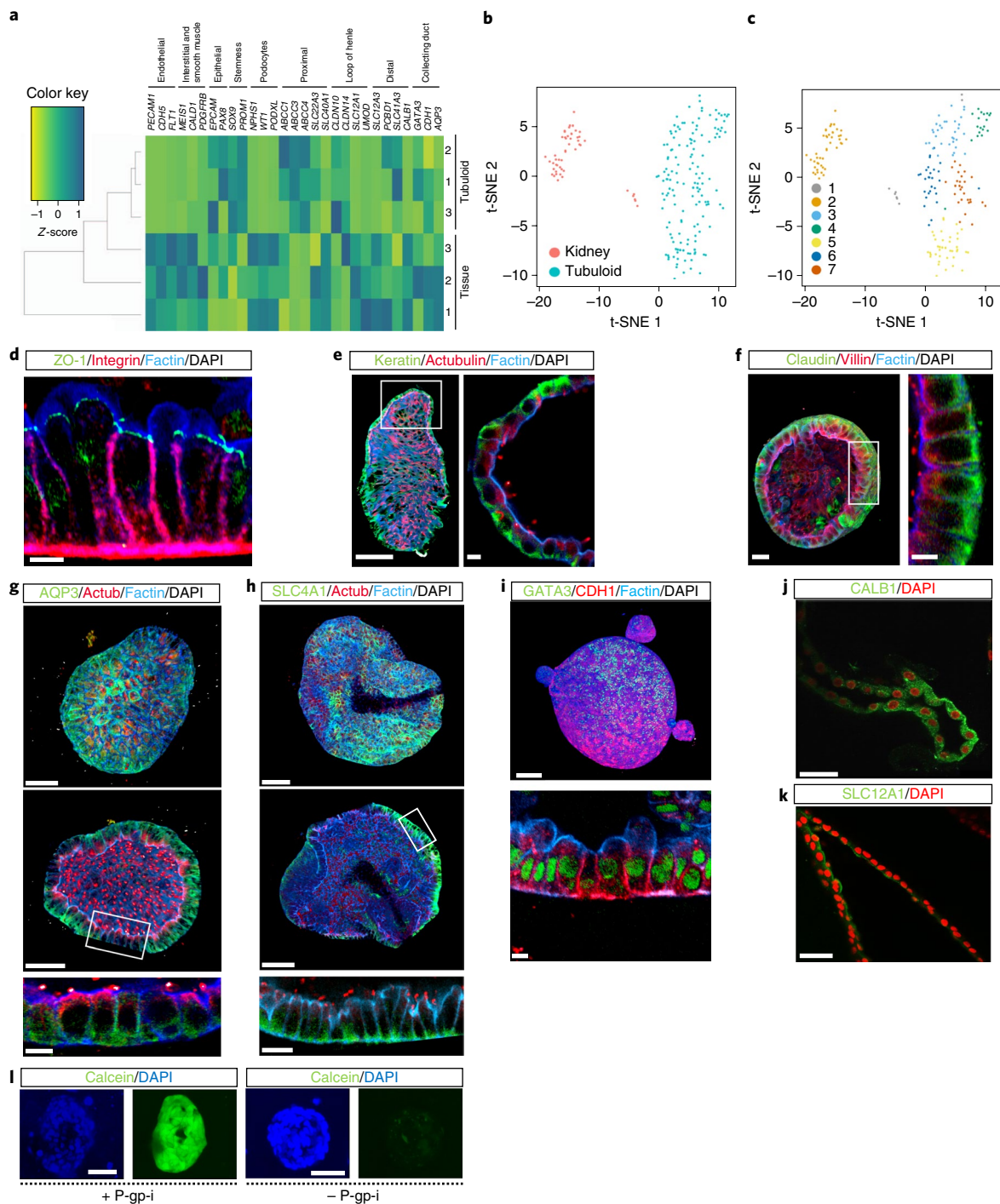
Immunostaining confirmed the tubular epithelial nature of the tubuloids. All tubuloids were *PAX8*⁺ (Supplementary Fig. 5). Basolateral Integrin $\alpha 6$ (ITGA6), sub-apical TJP1 (ZO1) and Filamentous-Actin (F-Actin) demonstrated that the structures form a polarized epithelium (Fig. 2d). This was further substantiated with basolateral cytokeratin (wide spectrum) combined with apical acetylated tubulin (to stain for the primary cilium; TUBA) and F-Actin (Fig. 2e). A three-dimensional reconstruction that illustrates the epithelial architecture, high level of polarization and the presence of an apical primary cilium on each tubuloid cell is provided in Supplementary Video 1. Proximal tubule cells were identified by Villin (VIL1), expressed in the microvilli of the proximal tubule, combined with basolateral Claudin-3 (*CLDN-3*) and F-Actin (Fig. 2f). In addition, we detected tubuloids that were positive for the principal cell marker of the collecting duct *AQP3* (Fig. 2g) and the intercalated cell marker *SLC4A1* (Fig. 2h). To confirm the presence of collecting duct cells, an immunofluorescent staining for *CDH1* and *GATA3* was performed, showing double-positive cells (Fig. 2i).

The bulk and single-cell RNA-seq analyses showed limited expression of loop of Henle-specific genes (*UMOD*, *SLC12A1*) and of the distal tubule marker *CALB1* (Fig. 2a and Supplementary Fig. 7). Indeed, *SLC12A1* was present in a minority of cells at the protein level at the apical side, where it is located in vivo (Fig. 2k). Growth factor withdrawal, a method previously used to promote differentiation of other types of organoids³⁹, allowed detection of distal tubule marker *CALB1* in the cytoplasm and loop of Henle marker *UMOD* by immunofluorescence (Fig. 2j and Supplementary Fig. 7). When cells within a tubuloid were positive for a segment-specific marker, generally the majority of the cells in that tubuloid were positive for that marker (Fig. 2f–j), suggesting a nephron segment-specific phenotype of individual tubuloids.

Fig. 2 | Kidney tubuloids represent tubular epithelium. **a**, Color-coded heatmap of an RNA-seq analysis comparing 3 independent cortical tissue samples (1, 2, 3) and the 3 corresponding tubuloid lines (1, 2, 3), showing that tubuloids are tubular epithelial in nature, have a high expression of ASC markers and express marker genes of proximal tubule, loop of Henle, distal tubule and collecting duct. **b**, *t*-distributed stochastic neighbor embedding (*t*-SNE) maps of unsupervised clustering of matching primary kidney epithelial cells and cultured tubuloid cells (192 kidney and 192 tubuloid cells were sequenced in one run and after quality checks (see Methods) 51 kidney cells and 149 tubuloid cells were used for clustering analysis). **c**, Seven clusters were identified: cluster 1 ($n = 8$) contains tubuloid and primary kidney epithelial cells and these cells express typical intercalated cell genes; cluster 2 ($n = 45$) contains only primary kidney epithelial cells, whereas cluster 3–7 contains only tubuloid-derived cells. Cluster 4 ($n = 19$) expresses collecting duct genes, cluster 5 ($n = 39$) proximal tubule genes and cluster 7 ($n = 28$) displays a more fibrotic signature. Clusters 3 ($n = 33$) and 6 ($n = 28$) may represent a more undifferentiated progenitor phenotype (**c**). **d**, Immunofluorescent staining for basolateral Integrin $\alpha 6$, sub-apical ZO1 and F-Actin demonstrates that the tubuloids form a polarized epithelium (this combined staining was performed in one tubuloid line). **e**, Immunofluorescent staining for basolateral keratin combined with apical acetylated tubulin (primary cilium) and F-Actin confirms the polarized nature of the tubuloids (this combined staining was performed in one tubuloid line). **f**, Expression of Villin, a marker of the microvilli of the proximal tubule, is detected with immunofluorescence, in a staining combined with basolateral Claudin-3 and F-Actin (this combined staining was performed in one tubuloid line). **g,h**, The presence of collecting duct marker genes is detected with immunofluorescence: principal cell marker *AQP3* ($n = 3$ independent experiments) (**g**) and intercalated cell marker *SLC4A1* ($n = 3$ independent experiments) (**h**). **i**, Combined expression of *GATA3* and *CDH1* confirms the presence of collecting duct cells ($n = 3$ independent experiments). **j**, Expression of distal tubule marker *CALB1* is observed after withdrawal of growth factors ($n = 2$ independent experiments). **k**, A minority of the tubuloid cells express loop of Henle marker *SLC12A1* ($n = 2$ independent experiments). **l**, Tubuloids display proximal tubule transporter function: by addition of a P-gp-specific inhibitor (+ P-gp-i), accumulation of calcein (Calc) is observed. This is not observed without the inhibitor (– P-gp-i) ($n = 3$ independent experiments). Scale bars, 50 μm , except **d** and insets in **e, f, g, h, i** where it is 10 μm .

To evaluate functionality of the proximal tubule cells, we exposed tubuloids to a substrate (calcein-AM, which diffuses freely into cells) of the proximal tubule xenobiotics efflux pump ABCB1 (P-glycoprotein (P-gp)) in the presence or absence of the P-gp-specific inhibitor PSC-833 (ref. 40). If P-gp were functional in tubuloids, accumulation of calcein-AM (which is intracellularly cleaved into the fluorescent calcein) should occur when P-gp-activity is blocked. An illustration of the experimental set-up is provided in Supplementary Fig. 8. We observed accumulation of calcein in the presence of the inhibitor as assessed by confocal microscopy (Fig. 2l). We quantified this by measuring fluorescence in a plate reader and found the difference to be significant ($P=0.0016$, Supplementary Fig. 9).

A defining feature of stem cells is their multilineage potential⁴¹. We evaluated the presence of stem cells in the cultures by establishing a tubuloid line from a single cell. This clonal line expressed marker genes of multiple nephron segments, indicating multilineage capacity and hence stemness (Supplementary Fig. 10). In comparison with the bulk tubuloid line from which the clonal line was established, diversity in segments was largely preserved, although there were differences: the clonal tubuloid line had an increased expression of the traditional loop of Henle marker (*SLC12A1*) and a decreased expression of the typical distal tubule marker (*SLC12A3*). In addition, expression of the collecting duct marker *AQP3* was low while the other collecting duct marker *NR3C2* was only marginally increased compared to control colon organoids (both in the clonal



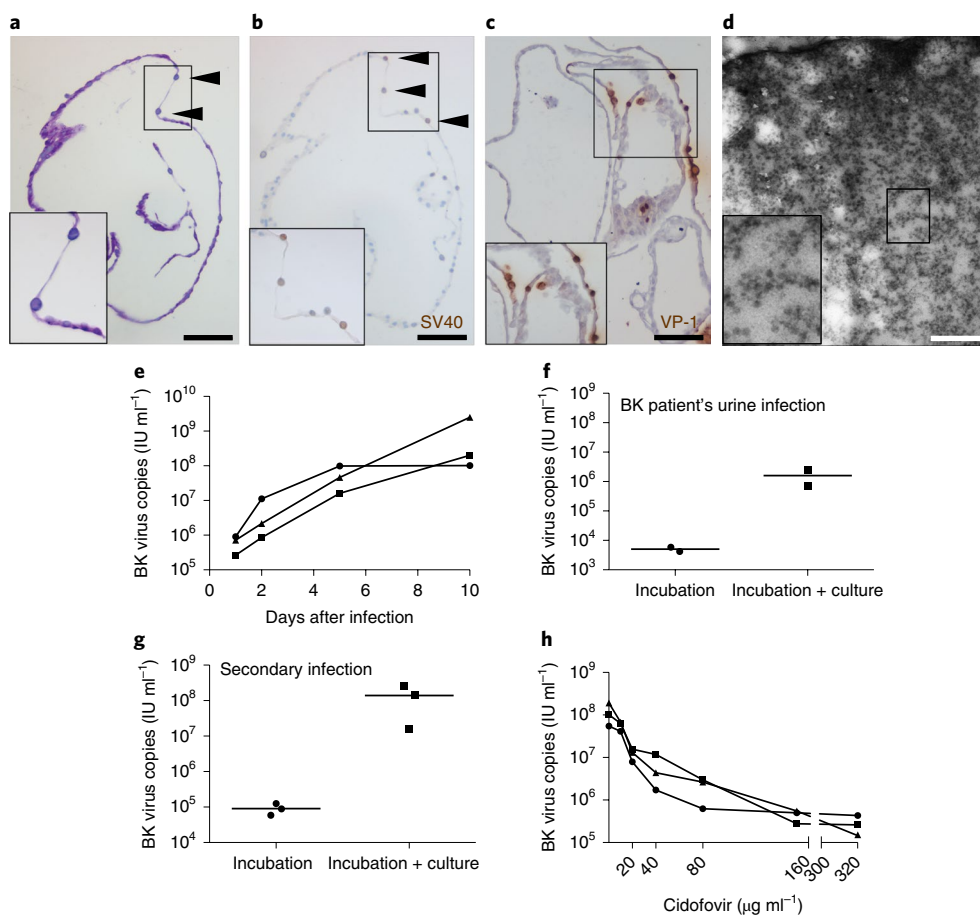


Fig. 3 | Modeling BK virus infection with human kidney tubuloids. a, Periodic acid-Schiff (PAS) staining reveals large blue nuclei (intranuclear basophilic viral inclusions; arrow heads) in an infected tubuloid 10 d post-infection ($n=2$ independent experiments). **b**, The larger nuclei (arrow heads) present in a patchy pattern 10 d post-infection, stain for SV40 T antigen ($n=2$ independent experiments). **c**, In addition, in the same tubuloid nuclei are present that stain for VP-1 10 d post-infection (experiment performed once). **d**, Transmission electron microscopy reveals the presence of viral particles in nuclei of an infected cell 10 d post-infection, and these were absent in the negative control (experiment performed once). **e**, BK virus particles increase exponentially in the first 10 d in culture (each line represents one independent experiment, data expressed genome equivalents in International Units per ml). **f**, Infection of tubuloids can be established directly from urine from a patient with BK virus-induced nephropathy: the number of virus particles increases sharply between the start of incubation (Incubation) and after 10 d of culture (Incubation + culture) (each dot represents an independent experiment ($n=2$), the line indicates the mean, data expressed as genome equivalents in International Units per ml). **g**, Filtered supernatant of tubuloids infected with BK virus is infectious: we compared input (Incubation) to the output after culture (Incubation + culture) (each dot represents an independent experiment ($n=3$), the line indicates the mean, data expressed as genome equivalents in International Units per ml). **h**, The number of BK virus copies decreases significantly in the presence of CDV in a dose-dependent manner (each line represents one independent experiment, data expressed as genome equivalents in International Units per ml; $P < 0.01$ from $20 \mu\text{g ml}^{-1}$ onwards, using a one-way analysis of variance (ANOVA), combined with Tukey post-hoc tests). Scale bars, **a-c**, $100 \mu\text{m}$; **d**, 500nm .

and parental lines). This suggested the lack of collecting duct cells in the clonal line. Together, this indicated that the clonal line displayed a proximal nephron (proximal tubule and loop of Henle) phenotype, rather than a distal nephron (distal tubule and collecting duct) phenotype. Yet, we deduced from this that tubuloids contain cells with multilineage potential, designating them as ASCs.

Thus, in tubuloids under expansion conditions, proximal tubule cells were abundantly present and functional, collecting duct cells were more sparsely present and a few loop of Henle cells were found.

Modeling infectious kidney disease. BK virus is a tubule-specific circular DNA virus for which no curative treatment exists. To validate tubuloids as an ex vivo model to study BK virus infection, we infected kidney tubuloids with a clinical isolate of BK virus that was first propagated in a cell line. Scattered nuclei of tubuloid cells increased to at least twice the normal size (Fig. 3a). The enlarged nuclei stained strongly for SV40/Large T antigen, which is used to

diagnose BK nephropathy in kidney biopsies (Fig. 3b). At the same time point post-infection (10 d), in the same tubuloid, enlarged nuclei were present that stained for VP-1 (Fig. 3c), showing that both early (SV40/Large T antigen) and late (VP-1) genes of BK virus were expressed at that time point. The presence of large numbers of viral particles within the nuclei was confirmed by transmission electron microscopy (Fig. 3d). The number of virus copies increased exponentially during the first 10 d after infection (Fig. 3e) as shown by quantitative PCR. In addition to productive infection with a clinical isolate propagated in a cell line, infection could be established from urine samples of a BK virus patient (Fig. 3f). In three experiments, viral DNA was sequenced at day 1 and day 30 after infection of tubuloids; no DNA changes were detected (sequencing data in Supplementary Dataset 3). Negative controls were included in all experiments to rule out that a latent BK virus strain replicated rather than the added strain. Thus, BK virus expands stably in human kidney tubuloids.

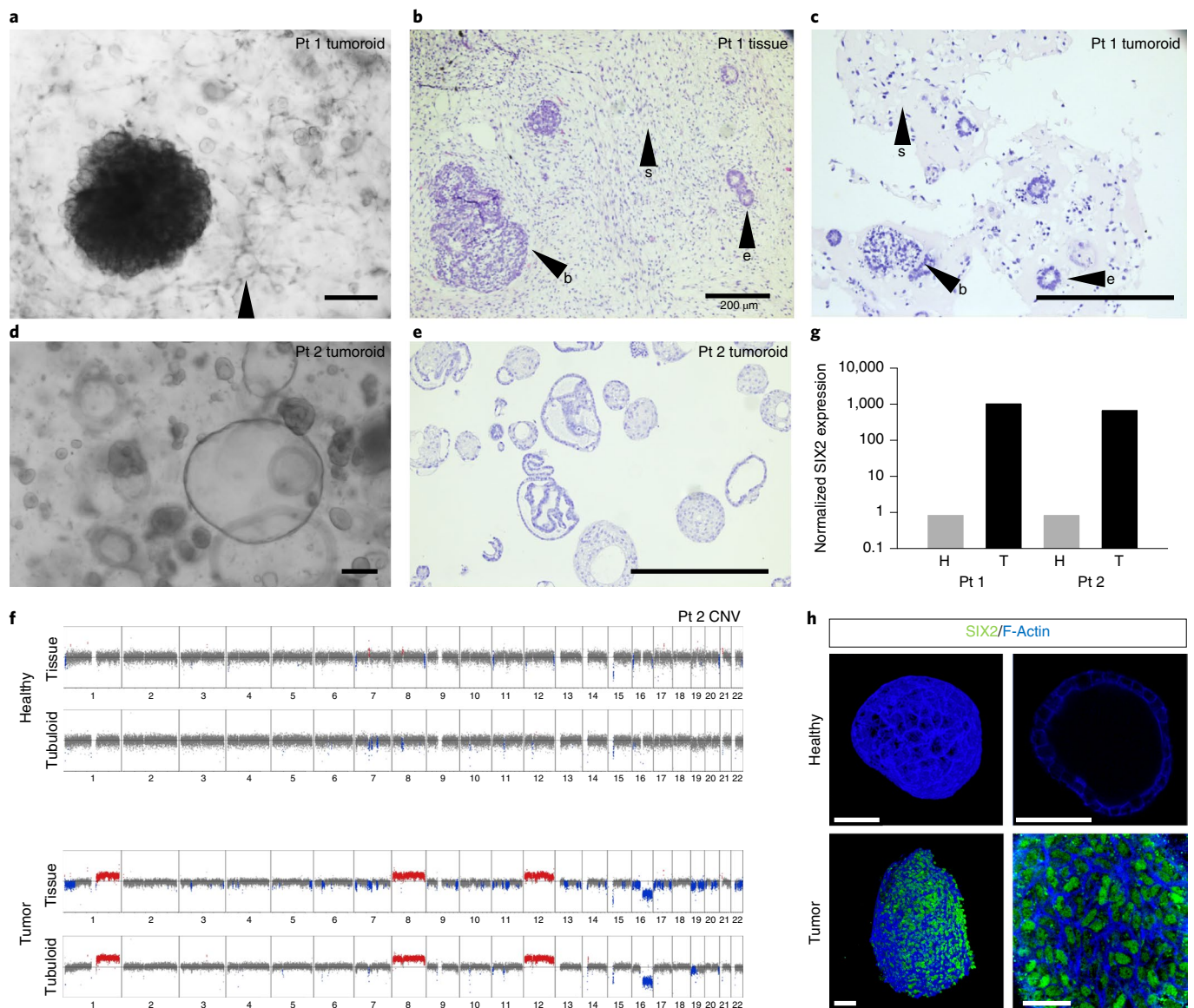


Fig. 4 | Tumoroid lines can be established from Wilms tumor tissue. **a**, Nephroblastoma-derived tumoroids of patient 1 (Pt1), as assessed with bright field microscopy (representative image of at least $n=3$ independent experiments) that shows expansion of the stromal (arrow head) compartment of the tumor (Supplementary Videos 2–4). **b,c**, Hematoxylin and eosin (H&E) stains (performed once for this tumoroid line) of the primary tumor tissue (**b**) and the tumoroid line (**c**) both show the typical tri-phasic nephroblastoma histology, with blastema (arrow head b), epithelium (arrow head e) and stroma (arrow head s) present. **d,e**, The second nephroblastoma (Pt2) did not show this tri-phasic morphology: bright field (representative image of at least $n=3$ independent experiments) (**d**) and H&E staining (performed once for this tumoroid line) (**e**). **f**, Low-coverage WGS of patient 2 (experiment performed once) shows that healthy tissue and the healthy tubuloid line do not display CNVs. However, in the tumor tissue and tumoroid line, typical Wilms tumor CNVs, such as 1q gain, gain of chromosome 8 and 12, and 16q loss were identified. **g**, Wilms tumor-derived tumoroids (T) from both patients express *SIX2*, whereas the matched normal lines (H) do not: normalized expression is depicted (analysis performed in triplicate for $n=2$ independent lines, once). **h**, This is confirmed with immunofluorescence staining for *SIX2* and F-Actin (representative image of $n=3$ independent experiments). Scale bars, 200 μm , except **h** where it is 50 μm .

To test whether virus particles produced in culture were infectious, we filtered culture supernatant 30 d after tubuloid infection. As the medium was refreshed 13 times, there was a minimal contribution of virus particles used to establish infection. Incubation of tubuloids with the filtered supernatant was sufficient to establish infection and subsequent culturing increased the number of viral copies (Fig. 3g), indicating active production of infectious viral particles. We tested the effect of anti-viral treatment by incubating tubuloids with BK virus and culturing them for 7 d in the presence of 10–320 $\mu\text{g ml}^{-1}$ cidofovir (CDV; an inhibitor of DNA polymerase), a drug used clinically for the treatment of BK virus

nephropathy⁴². The number of viral copies decreased significantly compared to control ($P < 0.01$, from 20 $\mu\text{g ml}^{-1}$ onwards) in a dose-dependent manner (Fig. 3h). The half-maximum inhibitory concentration ($\sim 10 \mu\text{g ml}^{-1}$) was within the range of clinically obtained serum levels⁴³. Thus, BK virus infection in tubuloids mimics clinical histopathology with respect to the patchy pattern of infection and histological findings and allows testing of treatment efficacy *ex vivo*.

Establishing ‘tumoroids’ from Wilms tumors. Wilms tumor, or nephroblastoma, is the most common pediatric solid tumor, accounting for 5% of all childhood malignancies⁴⁴. Mutations in

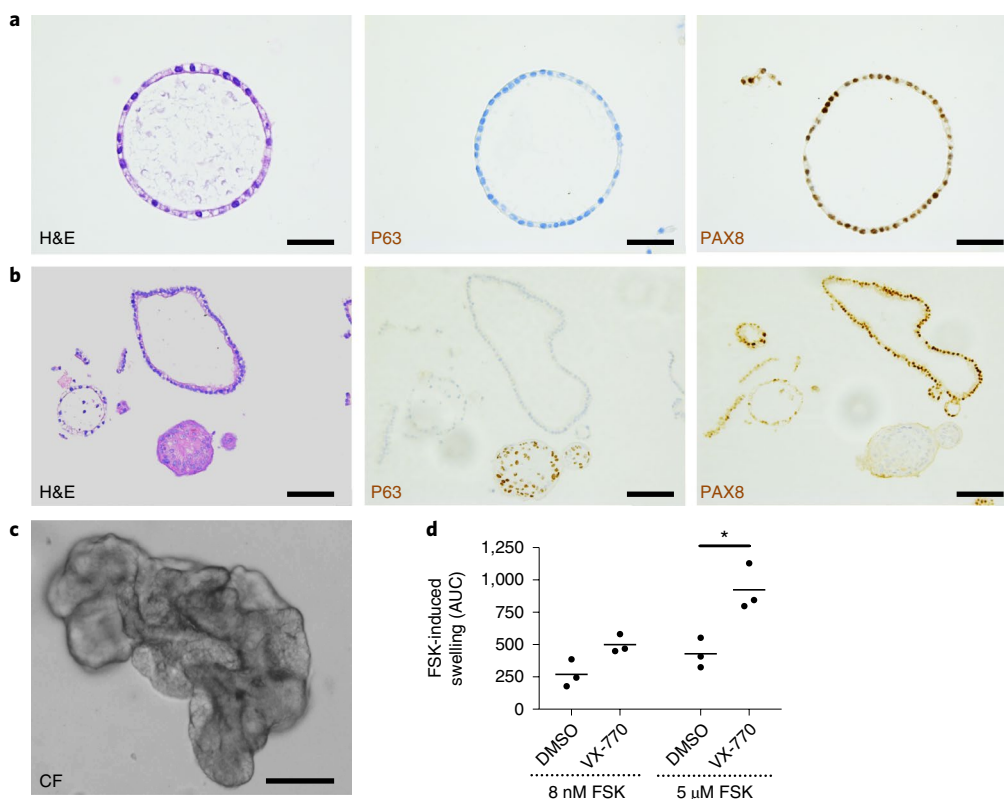


Fig. 5 | Tubuloid lines from urine allow CF response assessment. **a**, Urine-derived tubuloids can originate from kidney epithelium, as demonstrated with PAX8⁺ staining (performed in $n = 4$ independent lines). **b**, Occasionally, urothelium-derived (P63⁺ PAX8⁻) organoids are also observed (performed in $n = 4$ independent lines; P63⁺ PAX8⁻ cells were present in one line). **c**, Typical phenotype of urine-derived CF kidney tubuloids after 10 passages (representative image of least $n = 3$ time points). **d**, CF-urine tubuloids do not swell significantly in response to forskolin (FSK, 8 nM and 5 μM) when preincubated with dimethylsulfoxide (DMSO), but swelling can be significantly increased by the CF drug VX-770 (means of $n = 3$ independent experiments are plotted, each dot represents an experiment, AUC: area under the curve). * $P = 0.02$ with a two-tailed unpaired t -test. Scale bars, 100 μm.

genes such as *WT1*, *CTNBN1* or *SIX2* are believed to occur in kidney stem or progenitor cells during embryonic development. The resulting Wilms tumors often display a typical tri-phasic histology, with stroma, blastema and epithelium as components⁴⁵. Copy number variations (CNVs) are observed in 75% of cases^{46,47}. In addition, expression of the kidney developmental stem cell marker *SIX2* is observed⁴⁸.

We established tumor organoids, or ‘tumoroids’, from tumor and matching normal tissue of two patients with nephroblastoma (Fig. 4a,d). Nephroblastoma tumoroids from both patients could be expanded with a split ratio of 1:2–1:3 once every 10–14 d. The tumor tissue of the first nephroblastoma patient contained stroma, blastema and epithelium. The tumor-derived structures displayed a clearly different morphology compared to tubuloids derived from healthy tissue, as assessed by phase-contrast microscopy (Fig. 4a) and 6-day time-lapse imaging videos (Supplementary Videos 2–4). The most striking difference was the presence of a stromal (non-epithelial) compartment in culture. Like the original tumor tissue (Fig. 4b), the tumoroids contained stroma, blastema and epithelium (Fig. 4c). An 8-base-pair deletion was found in Exon 7 of *WT1*, present in all healthy and tumor-derived samples, implying a germline mutation in *WT1* (Supplementary Fig. 11a). An additional heterozygous 4-base-pair Exon 10 insertion was found in tumor tissue as well as in the tumoroids. This mutation was acquired as it was absent from healthy tissue and healthy tubuloids (Supplementary Fig. 11b).

In the case of the second patient, the tumor-derived structures were morphologically similar to healthy tissue-derived tubuloids (Fig. 4d,e). However, low-coverage WGS revealed typical CNVs

associated with nephroblastoma, including gains of 1q and of chromosomes 8 and 12 (ref. ⁴⁹) and loss of 16q⁵⁰. Identical CNVs were found in the primary tumor tissue (Fig. 4f) but not in the healthy tissue and the healthy tubuloids, proving that the tumoroids genetically reflected the primary tumor.

Wilms tumors often highly express *SIX2*, particularly those that do not carry *SIX2* driver mutations⁴⁸. From the RNA-seq analysis described above, we confirmed that adult kidney tissue and healthy tubuloids do not express *SIX2*. Accordingly, the tubuloids derived from the healthy kidney tissue of the two Wilms tumor patients did not express *SIX2*, while *SIX2* expression was sharply upregulated in both patients’ tumoroids (Fig. 4g,h).

Tubuloids from urine of individuals with cystic fibrosis. A limitation of the described culture system is that nephrectomy or biopsy is required to establish cultures. These invasive procedures are standard-of-care for only a limited number of kidney diseases. Using previously described protocols⁵¹, we were able to isolate cells from urine that could be expanded into tubuloids. Urine-derived kidney tubuloid lines could be expanded over 10–15 passages with weekly passaging in a 1:3 ratio. We established three independent tubuloid lines from healthy volunteers (two pediatric and one adult). Tubuloid cultures were derived from kidney epithelium, as demonstrated by PAX8⁺ staining of all tubuloids in two lines (Fig. 5a). One line contained a mixed culture of PAX8⁺ and PAX8⁻ structures, the latter positive for the urothelial marker TP63 (P63) (Fig. 5b).

In addition, we established a tubuloid line from urine of a patient with cystic fibrosis (CF) (carrying the *CFTR* mutations F508del/

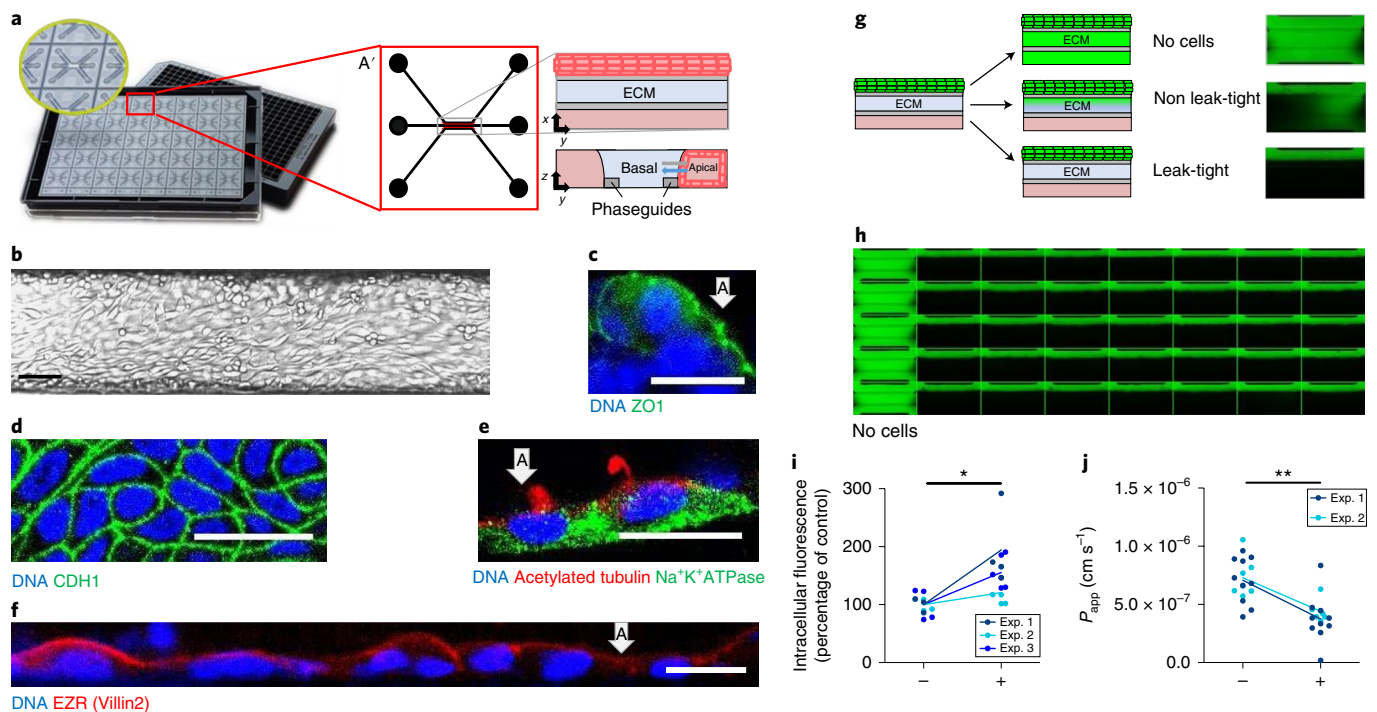


Fig. 6 | Tubuloid cells form tubes on organ-on-a-chip plates. **a**, The OrganoPlate platform with 40 microfluidic cell culture chips embedded in a standard 384-well microtiter plate. Schematic layout of one chip on the organ-on-a-chip plate, with separate compartments for gel and medium perfusion with cells seeded in one medium channel (A'). **b**, Seven days after seeding, a confluent tubular layer is formed as assessed by bright field microscopy ($n \geq 3$ independent experiments with up to $n = 40$ tubes per experiment). **c, d**, Immunofluorescence shows cells that express ZO1, a marker for tight junctions that is located sub-apically (representative image of $n = 3$ independent experiments with at least 3 replicates) (**c**) and E-Cadherin (CDH1), a marker for the adherens junctions (representative image of $n = 3$ independent experiments with at least 3 replicates) (**d**). **e**, Immunofluorescence shows cells that are positive for acetylated tubulin on the apical side and Na^+/K^+ -ATPase on the basolateral side, showing that the cells are polarized (representative image of $n = 3$ independent experiments with at least 3 replicates). **f**, Immunofluorescence shows cells that are positive for Ezrin, a marker for the microvilli on the apical side of proximal tubule cells (representative image of $n = 3$ independent experiments with at least 3 replicates). **g**, Schematic layout of a barrier integrity assay, where FITC-dextran is added to the lumen of the cell compartment ($n = 3$ independent experiments). In chips with tube formation, no leakage is observed, whereas in the negative control (no cells present), FITC-dextran spreads over the whole chip. **h**, A typical organ-on-a-chip plate overview after 20 min of 20 kDa FITC-dextran exposure, where FITC-dextran spreads over the whole chip in the negative controls (no cells, first column), but not in the chips where cells were plated (representative image of $n = 3$ independent experiments). **i**, The tubes significantly increase in intracellular calcein, after inhibition of P-gp with PSC-833, demonstrating P-gp activity (individual tubes are plotted, after normalization of $n = 3$ experiments (Exp.) and the lines indicate the mean per experiment; * $P = 0.03$ with a two-tailed unpaired t -test). **j**, Fluorescent rhodamine 123, which was added at the basal side of the tubes, is detected in the lumen at the apical side and the apparent permeability (P_{app}) can be reduced by the addition of PSC-833, demonstrating that the process is P-gp-dependent. Means of technical duplicates are plotted of $n = 2$ independent experiments; lines indicate the mean per experiment; ** $P = 0.00001$ with a two-tailed unpaired t -test. Immunofluorescent images (**c, e, f**) are a z-slice of the tube and positioned at $50 \mu\text{m}$ from the bottom glass, whereas **d** is positioned on the bottom glass. White arrows (**c, e, f**) indicate the apical side of the tube. Scale bars, **b**, $100 \mu\text{m}$; **c-f**, $25 \mu\text{m}$.

S1251N), from which an intestinal organoid line had already been established. These tubuloids were PAX8⁺ (Supplementary Fig. 12) and thus kidney-derived. Morphologically, the kidney tubuloids remained folded over long-term culture (~ 10 passages) (Fig. 5c), rather than the typical cystic phenotype (Fig. 5a). This is analogous to the morphology of intestinal CF organoids, which are also folded, while normal intestinal organoids are cystic⁶. This difference in phenotype between CF and normal organoids/tubuloids (described in more detail in ref.⁶) is probably a result of the lack of CFTR function, which reduces the flow of chloride into the lumen of the organoids and consequently reduces the amount of water that follows by osmosis.

We evaluated whether tubuloids are useful for testing CF treatment efficacy by performing the previously described forskolin swelling assay⁵, which is currently being used with rectal organoids as an ex vivo drug efficacy screen in the clinical management of CF in the Netherlands^{6,52}. The addition of forskolin, which opens the CFTR channel, leads to rapid swelling of healthy intestinal organoids and no swelling of CF rectal organoids. With certain specific mutations, such as F508del/S1251N⁶, some CFTR function remains.

A strong correlation exists between restoration of the swelling response by CFTR-restoring drugs and the clinical response of individual patients⁶.

In CF-urine tubuloids, forskolin caused minimal swelling (Supplementary Video 5) in a concentration-dependent manner (8 nM and $5 \mu\text{M}$; Fig. 5d), indicating some residual CFTR function, which is expected with the F508del/S1251N genotype⁶. Swelling increased significantly ($P = 0.02$ with $5 \mu\text{M}$ forskolin) by pre-incubation with the CFTR-potentiator drug VX-770 (ivacaftor, Kalydeco) (Supplementary Video 6), a registered drug for treatment of F508del/S1251N mutations that also clinically benefitted this patient (Fig. 5d). The intestinal organoids from the same patient yielded similar results to the CF-urine tubuloids: forskolin induced limited swelling (Supplementary Video 7), which was enhanced by pre-incubation with the CF drug VX-770 (Supplementary Fig. 13 and Supplementary Video 8).

Tubuloids-on-a-chip. Previously, proximal tubule cell lines have been coerced into a kidney tubule conformation⁵³. To guide tubuloids

to grow in a kidney tubule conformation, we plated tubuloid-derived cells in a three-lane OrganoPlate⁵⁴, an organ-on-a-chip platform with 40 parallel chips having stratified compartments for extracellular matrix (ECM) and medium perfusion (Fig. 6a). Tubules are cultured in a medium perfusion compartment along the matrix gel allowing apical as well as basolateral access⁵⁵. After seeding, tubes formed within 7 d (Fig. 6b) and the cells building the tubes were polarized, as assessed by immunofluorescence of acetylated tubulin (apical) and Na⁺/K⁺-ATPase (AT1A1, basolateral) (Fig. 6e). In addition, cells expressed the proximal tubule microvillus marker Ezrin (EZR) apically (Fig. 6f), whereas CDH1 showed the presence of adherens junctions (Fig. 6d). ZO1 expression (Fig. 6c) visualized tight junctions and suggested leak-tightness of the tubes. To confirm that the tubules were leak-tight, we added 20kDa fluorescein isothiocyanate-(FITC-)dextran and 155kDa tetramethylrhodamine isothiocyanate-(TRITC-) dextran to the cell compartment (Fig. 6g,h). After 20 min, FITC-dextran remained within the cellular tube compartment, whereas in the negative control (no cells plated), FITC-dextran was diffusely present throughout all compartments (Fig. 6h).

As tubes were leak-tight, we performed a P-gp transporter assay in the presence or absence of inhibitor PSC-833 as described above (Fig. 2l and Supplementary Figs. 8 and 9). We observed a significant ($P=0.03$) accumulation of calcein intracellularly in the presence of PSC-833, demonstrating activity of P-gp (Fig. 6i). Subsequently, we tested whether the tubes displayed trans-epithelial transport function. Fluorescent rhodamine 123 is transported into cells by Organic Cation Transporter 1 and 2 (OCT1 and OCT2)⁵⁶, which are influx pumps located on the basolateral side of proximal tubule cells. It is secreted from cells at the apical membrane by P-gp⁵⁷. Rhodamine 123 was added at the basal side of the tube in the presence or absence of the P-gp inhibitor PSC-833. After 3 and 5 h of incubation, the fluorescent intensity of rhodamine 123 at the apical side was measured and the difference between the two time points was quantified and used to calculate the apparent permeability (P_{app}). A scheme of the experimental set-up is provided in Supplementary Fig. 14. Fluorescence was detected at the apical side, indicating trans-epithelial transport (Fig. 6j). The apparent permeability was reduced in the presence of PSC-833 ($P=0.00001$), showing that efflux of rhodamine 123 was dependent on P-gp function (Fig. 6j).

Thus, tubuloid-derived cells can form leak-tight, polarized kidney tubules that can perform (trans-epithelial) transporter activity in an organ-on-a-chip format, enabling personalized transporter and drug-disposition studies in tubuloids.

Discussion

In this study, we report a robust kidney tubuloid culture system that allows long-term expansion and analysis of healthy and diseased human kidney tissue. The technology is developed based on previous protocols for stable expansion of epithelial elements of a variety of ecto-, meso- and endodermal organs¹. These previous protocols have been used for a wide range of applications, as ASC-derived organoids can be subjected to essentially any experimental manipulation and analysis that has been established for classical cell lines. The expanding kidney tubuloids retain the characteristics of primary, functional renal epithelial cells representing distinct nephron segments, most notably of the proximal tubule. We demonstrate the use of tubuloids for the modeling of an infectious kidney disease (BK virus), a malignancy (Wilms tumor) and a hereditary disease (CF).

BK virus infections are responsible for the loss of 5–10% of donor organs in kidney transplant recipients⁵⁸. Currently, BK virus is studied using kidney cell lines, wherein a diffuse and general infection is observed⁵⁹. Infection of tubuloids yielded a patchy pattern of infection and an increase of nuclear volume (due to intranuclear basophilic viral inclusions⁶⁰), which mimics the findings in BK nephropathy kidney biopsies⁶¹. In addition, tubuloid culture allows the study of virus infection in a personalized fashion.

Methods to study patient-derived Wilms tumors have thus far involved cell lines and patient-derived xenografts. These xenografts are expensive, have a low 'take' rate, are slow to establish and are not amenable to high-throughput studies. The few existing Wilms tumor cell lines (for example, ref. ⁶²) have undergone extensive in vitro adaptation/selection. These cell lines do not yield the histology of typical Wilms' tumors, while Wilms tumoroids typically do: we present a Wilms tumoroid culture that contains the three components (stroma, blastema and epithelium) seen in a subset of Wilms tumors. An added advantage of the current technology is the availability of the original tumor tissue as well as of matching normal kidney tissue and tubuloids.

In the Netherlands, a Forskolin-based swelling assay on rectal organoids is used for determining treatment efficacy in CF. Tubuloid cultures established from urine might reduce the need for more invasive rectal biopsies. Because this proof-of-principle was established for a single patient, this application awaits further validation. Besides the use for CF, deriving tubuloid cultures from urine may also be valuable for the study of (rare) genetic kidney diseases, for which biopsies are not routinely taken.

We believe that our tubuloid culture system is complementary to the existing PSC-derived organoids^{63–66}. It adds the unique feature of direct expansion of patient-derived renal tissue (from biopsy material and from urine). It is thus very rapid and does not have the disadvantages of reprogramming to iPSCs, including genetic instability during long culture periods⁵⁷. There are, however, limitations to the culture system. First, the tubuloid cultures are heterogeneous. In a way, this is an advantage of the system, as the heterogeneity of the tubuloids may reflect the heterogeneity within the tubular epithelium. A strategy to mitigate heterogeneity is making clonal lines, which represent regional identities. For some studies this will be beneficial (for example, for studying a specific proximal tubule transporter) and for others it will be a drawback (for example, the study of renal tumor heterogeneity). Second, under the current culture conditions, we generate cells representing proximal tubules, loop of Henle, distal tubules and collecting duct. Yet, glomerular cells are lacking. As ASC-organoids recapitulate tissue repair and given that entire nephrons cannot be replaced, it was expected that glomerular cells cannot be expanded in this culture system. Third, while we are able to generate cells expressing markers of the different nephron compartments, the conditions are biased for proximal tubule cell generation. Future studies will address growth factor conditions to efficiently generate other parts of the nephron. Fourth, the culture system is purely epithelial in nature, and lacks interstitial cells and vasculature. Yet, it should be noted that epithelial cells are often the primary substrate of disease.

Taking together the present results, we have established a versatile culture system for primary kidney epithelial cells that allows molecular and cellular analyses, disease modeling and drug screening in a rapid and personalized fashion. Future studies may optimize specific growth factor (withdrawal) conditions to enrich for loop of Henle and distal tubule cell types, as has been done successfully for the various small intestinal epithelial cell types⁶⁸.

Online content

Any methods, additional references, Nature Research reporting summaries, source data, statements of data availability and associated accession codes are available at <https://doi.org/10.1038/s41587-019-0048-8>.

Received: 21 June 2017; Accepted: 23 January 2019;
Published online: 4 March 2019

References

1. Clevers, H. Modeling development and disease with organoids. *Cell* **165**, 1586–1597 (2016).

2. Drost, J. & Clevers, H. Organoids in cancer research. *Nat. Rev. Cancer* **18**, 407–418 (2018).
3. Takasato, M. et al. Kidney organoids from human iPS cells contain multiple lineages and model human nephrogenesis. *Nature* **526**, 564–568 (2015).
4. Sato, T. et al. Single Lgr5 stem cells build crypt-villus structures in vitro without a mesenchymal niche. *Nature* **459**, 262–265 (2009).
5. Dekkers, J. F. et al. A functional CFTR assay using primary cystic fibrosis intestinal organoids. *Nat. Med.* **19**, 939–945 (2013).
6. Dekkers, J. F. et al. Characterizing responses to CFTR-modulating drugs using rectal organoids derived from subjects with cystic fibrosis. *Sci. Transl. Med.* **8**, 344ra384–344ra384 (2016).
7. Sato, T. et al. Long-term expansion of epithelial organoids from human colon, adenoma, adenocarcinoma, and Barrett's epithelium. *Gastroenterology* **141**, 1762–1772 (2011).
8. Lancaster, M. A. et al. Impaired Wnt- β -catenin signaling disrupts adult renal homeostasis and leads to cystic kidney ciliopathy. *Nat. Med.* **15**, 1046–1054 (2009).
9. Adams, D. C. et al. Follistatin-like 1 regulates renal IL-1 β expression in cisplatin nephrotoxicity. *Am. J. Physiol. Renal Physiol.* **299**, F1320–F1327 (2010).
10. Poladia, D. P. et al. Role of fibroblast growth factor receptors 1 and 2 in the metanephric mesenchyme. *Develop. Biol.* **291**, 325–339 (2006).
11. Cancilla, B., Davies, A., Cauchi, J. A., Risbridger, G. P. & Bertram, J. F. Fibroblast growth factor receptors and their ligands in the adult rat kidney. *Kidney Int.* **60**, 147–155 (2001).
12. Xu, J., Lamouille, S. & Derynck, R. TGF- β -induced epithelial to mesenchymal transition. *Cell Res.* **19**, 156–172 (2009).
13. Watanabe, K. et al. A ROCK inhibitor permits survival of dissociated human embryonic stem cells. *Nat. Biotechnol.* **25**, 681–686 (2007).
14. Janda, C. Y. et al. Surrogate Wnt agonists that phenocopy canonical Wnt and β -catenin signalling. *Nature* **545**, 234–237 (2017).
15. Boj, S. F. et al. Organoid models of human and mouse ductal pancreatic cancer. *Cell* **160**, 324–338 (2015).
16. Baker, D. E. C. et al. Adaptation to culture of human embryonic stem cells and oncogenesis in vivo. *Nat. Biotechnol.* **25**, 207–215 (2007).
17. Cheng, L. et al. Low incidence of DNA sequence variation in human induced pluripotent stem cells generated by nonintegrating plasmid expression. *Cell Stem Cell* **10**, 337–344 (2012).
18. Cassio, D. Long term culture of MDCK strains alters chromosome content. *BMC Res. Notes* **6**, 162 (2013).
19. Olofsson, B. et al. Vascular endothelial growth factor B (VEGF-B) binds to VEGF receptor-1 and regulates plasminogen activator activity in endothelial cells. *Proc. Natl Acad. Sci. USA* **95**, 11709–11714 (1998).
20. Brunskill, E. W. et al. Atlas of gene expression in the developing kidney at microanatomic resolution. *Develop. Cell* **15**, 781–791 (2008).
21. Birukov, K. G. et al. Stretch affects phenotype and proliferation of vascular smooth muscle cells. *Mol. Cell. Biochem.* **144**, 131–139 (1995).
22. LeBleu, V. S. et al. Origin and function of myofibroblasts in kidney fibrosis. *Nat. Med.* **19**, 1047–1053 (2013).
23. Ozcan, A. et al. PAX 8 expression in non-neoplastic tissues, primary tumors, and metastatic tumors: a comprehensive immunohistochemical study. *Mod. Pathol.* **24**, 751–764 (2011).
24. Kang, H. M. et al. Sox9-positive progenitor cells play a key role in renal tubule epithelial regeneration in mice. *Cell Rep.* **14**, 861–871 (2016).
25. Bussolati, B. et al. Isolation of renal progenitor cells from adult human kidney. *Am. J. Pathol.* **166**, 545–555 (2005).
26. Barker, N. et al. Lgr5(+ve) stem/progenitor cells contribute to nephron formation during kidney development. *Cell Rep.* **2**, 540–552 (2012).
27. Kobayashi, A. et al. Six2 defines and regulates a multipotent self-renewing nephron progenitor population throughout mammalian kidney development. *Cell Stem Cell* **3**, 169–181 (2008).
28. Breiderhoff, T. et al. Deletion of claudin-10 (Cldn10) in the thick ascending limb impairs paracellular sodium permeability and leads to hypermagnesemia and nephrocalcinosis. *Proc. Natl Acad. Sci. USA* **109**, 14241–14246 (2012).
29. Dimke, H. et al. Activation of the Ca²⁺-sensing receptor increases renal claudin-14 expression and urinary Ca²⁺ excretion. *Am. J. Physiol. Renal Physiol.* **304**, F761–F769 (2013).
30. Ferrè, S. et al. Mutations in PCBD1 cause hypomagnesemia and renal magnesium wasting. *J. Am. Soc. Nephrol.* **25**, 574–586 (2014).
31. De Baaij, J. H. et al. Identification of SLC41A3 as a novel player in magnesium homeostasis. *Sci. Rep.* **6**, 28565 (2016).
32. Kriz, W. & Lehir, M. Pathways to nephron loss starting from glomerular diseases—insights from animal models. *Kidney Int.* **67**, 404–419 (2005).
33. Scialdone, A. et al. Computational assignment of cell-cycle stage from single-cell transcriptome data. *Methods* **85**, 54–61 (2015).
34. van den Brink, S. C. et al. Single-cell sequencing reveals dissociation-induced gene expression in tissue subpopulations. *Nat. Method* **14**, 935 (2017).
35. Karafin, M. et al. Diffuse expression of PAX2 and PAX8 in the cystic epithelium of mixed epithelial stromal tumor, angiomylipoma with epithelial cysts, and primary renal synovial sarcoma: evidence supporting renal tubular differentiation. *Am. J. Surg. Pathol.* **35**, 1264–1273 (2011).
36. Chen, G. New advances in urea transporter UT-A1 membrane trafficking. *Int. J. Mol. Sci.* **14**, 10674–10682 (2013).
37. Kirk, A., Campbell, S., Bass, P., Mason, J. & Collins, J. Differential expression of claudin tight junction proteins in the human cortical nephron. *Nephrol. Dial. Transplant.* **25**, 2107–2119 (2010).
38. Rudnicki, M. et al. Hypoxia response and VEGF-A expression in human proximal tubular epithelial cells in stable and progressive renal disease. *Lab. Invest.* **89**, 337–346 (2009).
39. Huch, M. et al. Long-term culture of genome-stable bipotent stem cells from adult human liver. *Cell* **160**, 299–312 (2015).
40. Jansen, J. et al. A morphological and functional comparison of proximal tubule cell lines established from human urine and kidney tissue. *Exp. Cell Res.* **323**, 87–99 (2014).
41. Barker, N., Van Oudenaarden, A. & Clevers, H. Identifying the stem cell of the intestinal crypt: strategies and pitfalls. *Cell Stem Cell* **11**, 452–460 (2012).
42. Ganguly, N. et al. Low-dose cidofovir in the treatment of symptomatic BK virus infection in patients undergoing allogeneic hematopoietic stem cell transplantation: a retrospective analysis of an algorithmic approach. *Transpl. Infect. Dis.* **12**, 406–411 (2010).
43. Cundy, K. C. et al. Clinical pharmacokinetics of cidofovir in human immunodeficiency virus-infected patients. *Antimicrob. Agents Chemother.* **39**, 1247–1252 (1995).
44. Kalapurakal, J. A. et al. Management of Wilms' tumour: current practice and future goals. *Lancet Oncol.* **5**, 37–46 (2004).
45. Rivera, M. N. & Haber, D. A. Wilms' tumour: connecting tumorigenesis and organ development in the kidney. *Nat. Rev. Cancer* **5**, 699–712 (2005).
46. Hohenstein, P., Pritchard-Jones, K. & Charlton, J. The yin and yang of kidney development and Wilms' tumors. *Genes Develop.* **29**, 467–482 (2015).
47. Hawthorn, L. & Cowell, J. K. Analysis of wilms tumors using SNP mapping array-based comparative genomic hybridization. *PLoS ONE* **6**, e18941 (2011).
48. Wegert, J. et al. Mutations in the SIX1/2 pathway and the DROSHA/DGCR8 miRNA microprocessor complex underlie high-risk blastemal type Wilms tumors. *Cancer Cell* **27**, 298–311 (2015).
49. Hing, S. et al. Gain of 1q is associated with adverse outcome in favorable histology Wilms' tumors. *Am. J. Pathol.* **158**, 393–398 (2001).
50. Mengelbier, L. H. et al. Deletions of 16q in Wilms tumors localize to blastemal-anaplastic cells and are associated with reduced expression of the IRXB renal tubulogenesis gene cluster. *Am. J. Pathol.* **177**, 2609–2621 (2010).
51. Zhou, T. et al. Generation of human induced pluripotent stem cells from urine samples. *Nat. Protoc.* **7**, 2080–2089 (2012).
52. Dekkers, J. F. et al. Potentiator synergy in rectal organoids carrying S1251N, G551D, or F508del CFTR mutations. *J. Cyst. Fibros.* **15**, 568–578 (2016).
53. Homan, K. A. et al. Bioprinting of 3D convoluted renal proximal tubules on perfusable chips. *Sci. Rep.* **6**, 34845 (2016).
54. Trietsch, S. J., Israëls, G. D., Joore, J., Hankemeier, T. & Vulto, P. Microfluidic titer plate for stratified 3D cell culture. *Lab Chip* **13**, 3548–3554 (2013).
55. Trietsch, S. J. et al. Membrane-free culture and real-time barrier integrity assessment of perfused intestinal epithelium tubes. *Nature Commun.* **8**, 262 (2017).
56. Juan, E., Vee, M., Denizot, C., Da Violante, G. & Fardel, O. The mitochondrial fluorescent dye rhodamine 123 is a high-affinity substrate for organic cation transporters (OCTs) 1 and 2. *Fundam. Clin. Pharmacol.* **28**, 65–77 (2014).
57. Yumoto, R. et al. Transport of rhodamine 123, a P-glycoprotein substrate, across rat intestine and Caco-2 cell monolayers in the presence of cytochrome P-450 3A-related compounds. *J. Pharmacol. Exp. Ther.* **289**, 149–155 (1999).
58. Hirsch, H. H. et al. Polyomavirus-associated nephropathy in renal transplantation: interdisciplinary analyses and recommendations. *Transplantation* **79**, 1277–1286 (2005).
59. de Kort, H. et al. Primary human renal-derived tubular epithelial cells fail to recognize and suppress BK virus infection. *Transplantation* **101**, 1820–1829 (2017).
60. Cakalagaoglu, F., Erbarut, I. & Tuglular, S. Frequency of BK virus nephropathy in graft dysfunction biopsies. *Dialysis Transplant.* **36**, 122–126 (2007).
61. Bohl, D. L. & Brennan, D. C. BK virus nephropathy and kidney transplantation. *Clin. J. Am. Soc. Nephrol.* **2**, S36–S46 (2007).
62. Royer-Pokora, B. et al. Wilms tumor cells with WT1 mutations have characteristic features of mesenchymal stem cells and express molecular markers of paraxial mesoderm. *Hum. Mol. Genet.* **19**, 1651–1668 (2010).
63. Takasato, M. et al. Directing human embryonic stem cell differentiation towards a renal lineage generates a self-organizing kidney. *Nat. Cell Biol.* **16**, 118–126 (2014).
64. Takasato, M. et al. Kidney organoids from human iPS cells contain multiple lineages and model human nephrogenesis. *Nature* **526**, 564–568 (2015).
65. Freedman, B. S. et al. Modelling kidney disease with CRISPR-mutant kidney organoids derived from human pluripotent epiblast spheroids. *Nat. Commun.* **6**, 8715 (2015).

66. Lam, A. Q. et al. Rapid and efficient differentiation of human pluripotent stem cells into intermediate mesoderm that forms tubules expressing kidney proximal tubular markers. *J. Am. Soc. Nephrol.* **25**, 1211–1225 (2014).
67. Gutierrez-Aranda, I. et al. Human induced pluripotent stem cells develop teratoma more efficiently and faster than human embryonic stem cells regardless the site of injection. *Stem Cells* **28**, 1568–1570 (2010).
68. Clevers, H. The intestinal crypt, a prototype stem cell compartment. *Cell* **154**, 274–284 (2013).

Acknowledgements

We thank the Hubrecht Imaging Center for assistance with (confocal) microscopy. We thank H. Begthel and J. Korving (both Hubrecht Institute) for preparation of histological and immunohistochemical specimens. We thank T. Nguyen (UMC Utrecht, the Netherlands) and R. de Krijger (Princess Máxima Center for Pediatric Oncology, Utrecht, the Netherlands) for help with the analysis of histological specimens. We thank the Hubrecht FACS facility for help with the sort of single (EPCAM+) cells and G. Posthuma (Department of Cell Biology and Institute of Biomembranes, UMC Utrecht, the Netherlands) for excellent support with transmission electron microscopy. We thank E. Driehuis for the photography of the VP-1 staining and for help with finalizing the manuscript. We thank J. Hoenderop (Radboud UMC, the Netherlands) for kindly providing UMOD and SLC12A1 antibodies, and NC3Rs for development of the kidney-on-a-chip assays (Nephrotube, CRACK-IT challenge). This work was supported by a grant from the Dutch Kidney Foundation (grant no. DKF14OP04), and Zwaartekracht (NWO). This work was supported by the partners of Regenerative Medicine Crossing Borders (www.regmedxb.com). Powered by Health–Holland, Top Sector Life Sciences & Health.

Author contributions

ES., M.B.R., M.C.V. and H.C. designed, performed, analyzed experiments and wrote the manuscript. C.A. established and maintained tubuloid cultures and performed

and analyzed karyotyping experiments. A.R. performed, imaged and analyzed immunofluorescent stainings. T.M. and F.H. analyzed the single-cell sequencing data. F.S., J.J. and R.M. designed, analyzed and performed the P-gp transporter assays in tubuloids. A.P.A.H. provided support with scanning electron microscopy images. F.S., M.Vi., M.B.R. and J.M. designed, performed and analyzed the BK virus experiments. R.v.B analyzed and interpreted the WGS analysis and E.C. gave input on the interpretation. B.A. helped with the analysis of the the bulk RNA-seq. M.M.H.E. established the logistics of obtaining clinical samples of nephroblastoma tissue. F.S. and J.D. established nephroblastoma cultures and designed experiments. E.H. performed and analyzed the nephroblastoma CNV analysis. S.D. established the clonal tubuloid line and F.Y.Y. analyzed the clonal tubuloid line. K.M.W.G. obtained CF urine samples. F.S., A.V. and J.B. designed FSK-induced swelling experiments and analyzed data. F.S., L.G., M.Vo. and H.L. designed, performed and analyzed the ‘tubuloid-on-a-chip’ experiments. All authors commented on the manuscript.

Competing interests

H.C. is a holder of several patents related to organoid technology. L.G., M.Vo. and H.L. are employees of MIMETAS BV, the Netherlands, that is marketing the OrganoPlate. OrganoPlate is a trademark of MIMETAS.

Additional information

Supplementary information is available for this paper at <https://doi.org/10.1038/s41587-019-0048-8>.

Reprints and permissions information is available at www.nature.com/reprints.

Correspondence and requests for materials should be addressed to H.C.

Publisher's note: Springer Nature remains neutral with regard to jurisdictional claims in published maps and institutional affiliations.

© The Author(s), under exclusive licence to Springer Nature America, Inc. 2019

Methods

Mice and human tissue. All animal experiments were approved by the Animal Experimentation Committee of the Royal Dutch Academy of Science and University Medical Centre (UMC) Utrecht and we complied with all relevant ethical regulations. All experiments with human tissue were approved by the medical ethical committee of the UMC Utrecht and we complied with all relevant ethical regulations. If required, written informed consent from patients was obtained.

Tubuloid culture. Human tissue. From cortical kidney tissue, tubular fragments were isolated by collagenase digestion (C9407, Sigma) for 45 min at 1 mg ml⁻¹. Fragments were seeded in growth factor-reduced Matrigel (Corning) or Basement Membrane Extract (BME, R&D Systems) and cultured in medium (ADMEM/F12 supplemented with 1% penicillin/streptomycin, HEPES, GlutaMAX, N-acetylcysteine (1 mM, Sigma) and 1.5% B27 supplement (Gibco)), supplemented with 10% Rspo1-conditioned medium⁶⁹ or 1% Rspo3-conditioned medium, the latter produced via the r-PEX protein expression platform (U-Protein Express), EGF (50 ng ml⁻¹, Peprotech), FGF-10 (100 ng ml⁻¹, Peprotech), Rho-kinase inhibitor Y-27632 (10 μM, Abmole), A8301 (5 μM, Tocris Bioscience) and primocine (0.1 mg ml⁻¹, Invivogen).

Differentiation medium contained ADMEM/F12 supplemented with 1% penicillin/streptomycin, HEPES and GlutaMAX.

Factors that were tested but that did not enhance expansion capacity were: 10% noggin-conditioned medium; 40% Wnt3a-conditioned medium (produced using stably transfected L cells), 0.5 nM Wnt-surrogates¹⁴ (U-Protein Express), 10 mM nicotinamide (Sigma), 3 μM p38-inhibitor (SB202190, Sigma), 1 μM PGE-2 (Tocris), 25 ng ml⁻¹ FGF-2 (Peprotech) and 10 ng ml⁻¹ BMP-4 (Peprotech).

Human urine. Urine (30–50 ml was sufficient) was processed quickly after voiding and, until processing, the sample was kept at 4 °C. Rho-kinase inhibitor Y-27632 (10 μM, Abmole) and primocine (0.1 mg ml⁻¹, Invivogen) were added. After centrifugation, the pellet was washed with medium (ADMEM/F12 supplemented with 1% penicillin/streptomycin, HEPES and GlutaMAX), supplemented with Rho-kinase inhibitor Y-27632 (10 μM, Abmole) and primocine (0.1 mg ml⁻¹, Invivogen). After a second centrifugation step, the pellet was resuspended in growth factor-reduced Matrigel (Corning) or BME (R&D Systems) and cultured in the tubuloid culture medium described above.

Clonal organoid line. Single-cell suspensions were generated from an early passage (P2) tubuloid line using TrypLE (Sigma-Aldrich). Single cells were sorted using FACS (FACS Aria, BD), resuspended in BME (R&D Systems) and plated in a limiting dilution. Cells were cultured in the described expansion medium. After approximately 4 weeks, single tubuloids were picked and clonally expanded as described.

Mouse. Kidneys were isolated and tubular fragments were isolated by collagenase digestion (C9407, Sigma) for 15 min at 0.5 mg ml⁻¹. Fragments were seeded in growth factor-reduced Matrigel (Corning) and cultured in medium (ADMEM/F12 supplemented with 1% penicillin/streptomycin, HEPES, GlutaMAX), with 1.5% B27 supplement (Gibco), 40% Wnt3a-conditioned medium (produced using stably transfected L cells), 10% noggin-conditioned medium, 10% Rspo1-conditioned medium⁶⁹, EGF (50 ng ml⁻¹, Peprotech), FGF-10 (100 ng ml⁻¹, Peprotech), N-acetylcysteine (1.25 mM, Sigma), A8301 (5 μM, Tocris Bioscience) and primocine (0.1 mg ml⁻¹, Invivogen).

Histology and immunohistochemistry. Tissues were fixed in 4% paraformaldehyde, dehydrated and embedded in paraffin. Sections were subjected to H&E, PAS and/or immunohistochemical staining. Immunohistochemistry was performed according to standard protocols on 3–4 μm sections. The primary antibodies were rabbit anti-Pax8 (1:500, 10336–1-AP, Proteintech), mouse anti-P63 (1:50, M7317, Dako), mouse anti-VP-1 (1:2,000, clone 3B2 SAB1412996, Sigma) and mouse anti-SV40 (1:100, bPAb416, Merck Millipore). Primary antibodies were dissolved in 0.05% BSA in PBS. If required, a rabbit-anti-mouse-HRP (1:500, Dako) in PBS and 5% normal mouse serum was used. Goat anti-rabbit PowerVision-Horse Radish Peroxidase (Leica Biosystems) was used as tertiary antibody and counterstaining was carried out with hematoxylin.

Scanning electron microscopy. Tubuloids were fixed for 15 min with 1% (v/v) glutaraldehyde (Sigma) in PBS at room temperature. Samples were subsequently serially dehydrated by consecutive 10 min incubations in 2 ml of 10% (v/v), 25% (v/v) and 50% (v/v) ethanol–PBS, 75% (v/v) and 90% (v/v) ethanol–H₂O, and 100% ethanol (2×), followed by 50% ethanol–hexamethyldisilazane (HMDS) and 100% HMDS (Sigma). The samples were removed from the 100% HMDS and air-dried overnight at room temperature. After overnight evaporation of HMDS, samples were mounted onto 12 mm specimen stubs (Agar Scientific) and coated with gold to 1 nm using a Quorum Q150R sputter coater at 20 mA before examination with a Phenom PRO Table-top scanning electron microscope (PhenomWorld).

Karyotyping. Tubuloids were treated with 0.1 μg ml⁻¹ colcemid (Gibco) for 16 h. Cultures were washed and dissociated into single cells using TrypLE (Gibco) and

processed as previously described⁷⁰. Slides were mounted with 4,6-diamidino-2-phenylindole (DAPI)-containing Vectashield and analyzed on a DM6000 Leica microscope. At least 40 spreads were analyzed, in at least three independent experiments, from multiple tubuloid lines.

Whole genome sequencing. DNA libraries for Illumina sequencing were generated by using standard protocols (Illumina) from 0.5 μg of genomic DNA isolated from tubuloid cultures by using the QIASymphony DSP DNA Mini Kit (Qiagen) according to manufacturer's instructions. All samples were sequenced (2 × 150 base pairs (bp)) by using Illumina HiSeq X Ten sequencers to 30× base coverage. Sequence reads were mapped and analyzed as previously described⁷¹. A full pipeline description and settings are available at <https://github.com/UMCUGenetics/IAP>. Raw variants were multisample-called by using the GATK HaplotypeCaller v.3.4–46 and postprocessing filters were performed as previously described⁷¹. Briefly, we considered variants at autosomal chromosomes without any evidence from a paired control sample (the original tissue used to generate the tubuloid cultures), passed by VariantFiltration with a GATK phred-scaled quality score ≥ 100, a base coverage of at least 20× in the control tissue, P2 and P8 cultures, a minimal variant allele frequency of 0.1, no overlap with single nucleotide polymorphisms in the Single Nucleotide Polymorphism Database v.137.b3730 and absence of the variant in a panel of unmatched normal human genomes (BED file available upon request). Finally, to obtain a final catalog of P2 mutations, we filtered variants with a GATK genotype score (GQ) lower than 99 in the P2 culture and 10 in the control sample. To obtain a final catalog of P8 mutations, we filtered variants with any presence in the P2 culture and with a GATK genotype score (GQ) lower than 99 in the P8 culture and 10 in the control sample and P2 culture. Sequence data have been deposited at the European Genome-phenome Archive (EGA), which is hosted by the EBI, under accession code EGAS00001002729.

Immunofluorescence. For whole mount immunofluorescence staining, tubuloids were processed as previously described⁷².

Rabbit anti-AQP-3 (1:100, 125219, Abcam), rabbit anti-AE1/SLC4A1 (1:100, AE11-A, Alpha Diagnostics International), goat anti-Calbindin D28K (1:200, N-18, Santa Cruz), goat anti-GATA3 (1:300, AF2605, R&D Systems), mouse E-Cadherin (1:300, 610182, BD Biosciences), rabbit anti-Claudin-3 (1:200, AB15102, Abcam), mouse anti-Integrin α6 (1:200, AB20142, Abcam), Alexa Fluor 647 Phalloidin (1:100, A22287, Thermo Fisher Scientific), mouse anti-Villin (1:200, SC-58897, Santa Cruz), rabbit anti-ZO1 (1:100, 402200, Thermo Fisher Scientific), mouse anti-acetylated tubulin (1:2,000, SC-23950, Santa Cruz), rabbit anti-cytokeratin (1:20, Z0622, Dako) and SIX2 (1:300, 11562–1-AP, Proteintech) were used as primary antibody. Sheep anti-UMOD (1:200) and rabbit anti-NKCC2 (1:200) were kindly provided by J. Hoenderop (Nijmegen, the Netherlands). Alexa Fluor immunoglobulin Gs (IgGs) were used as secondary antibodies: 568 donkey anti-rabbit IgG, Alexa Fluor 568 donkey anti-goat IgG, 488 donkey anti-rabbit IgG, 555 donkey anti-mouse IgG (1:500, Thermo Fisher Scientific). Nuclei were stained with DAPI (Thermo Fisher Scientific) or DRAQ5 (Biostatus). Immunofluorescence images were acquired using a confocal microscope (Leica, SP5 and SP8 or Zeiss LSM880). Images were analyzed and processed using Leica LAS AF Lite or LAS X software (Leica SP5 or SP8 confocal). Three-dimensional reconstruction of intact tubuloids was performed using the software Imaris.

Single-cell sequencing. Sample and SORT-seq library preparation. Samples were prepared according to the Sort-seq method as described previously⁷³. Briefly, EPCAM⁺ primary kidney cells, FACS sorted (Facsjazz, BD) with Alexa Fluor 488 anti-human CD326 (EPCAM, clone9C4; Biologend), and the single-cell suspension from passage 4 tubuloids (derived from the same tissue as the EPCAM⁺ primary kidney cells) were single-cell sorted into 384-well plates (Bio-Rad) containing 5 μl of vapor lock (Qiagen), 100–200 nl of reverse transcription (RT) primers, deoxyribose nucleoside triphosphates (dNTPs) and synthetic messenger RNA spike-ins.

Live single cells were selected on the basis of DAPI and forward/side scatter properties. After the sort, plates were spun down and frozen to –80 °C until further processing.

RNA samples were processed into complementary DNA libraries as described previously^{73,74} and on the basis of the CEL-seq2 technique. Illumina sequencing libraries were prepared with the TruSeq small RNA primers (Illumina) and were sequenced paired-end at 75-bp read length on an Illumina NextSeq. Primary cells and tubuloid cells were processed and sequenced in parallel.

Single-cell sequencing data analysis. Paired-end reads from Illumina sequencing were aligned to the human transcriptome with the Burrows-Wheeler Alignment (BWA) tool⁷⁵. Failed reactions as evident by lower external RNA controls counts were discarded. Cells with less than 2,000 unique transcripts were also removed. After cell filtering, unique transcript counts were normalized to 10,000, instead of down-sampling. Analysis was performed using the method of Satija et al.⁷⁶. Dissociation-induced stress³⁴ was quantified using a scoring strategy⁷⁷ based on the expression of heat shock genes (Supplementary Fig. 15). A score over 0.4 was used to filter out cells that were severely stressed. Cell-cycle analysis was performed as described before³³. To avoid clustering of cells based on cell-cycle profiles or stress,

the following genes were removed from the clustering estimation and included back for further analysis: the cell-cycle associated genes, heat shock protein genes, as well as genes assigned by curators (that is, not inferred from electronic annotation) with the gene ontology terms GO:0001666—response to hypoxia, GO:0006986—response to unfolded protein, GO:0006979—response to oxidative stress, GO:0006006—glucose metabolic process, GO:0006006—glucose metabolic process and GO:0042254—ribosome biogenesis. A total of 263 genes (18% of variable genes) were filtered out based on cell-cycle and gene ontology terms. The first 14 principal components were used for cluster identification with a resolution of 2. A pseudo-count of one was used. Differential expression was performed using the Wilcoxon test with 1.8-fold expression cut-off and 5% Bonferroni multiple-testing corrected statistical significance cut-off. Single-cell sequencing data can be found in the Supplementary Information and have been deposited at the Gene Expression Omnibus (GEO) under accession code [GSE107795](#).

Bulk RNA sequencing. Sample and library preparation. Passage 3 or 4 tubuloid samples ($n = 3$; 200 μ l of BME per sample) and matched cortical kidney tissue samples ($n = 3$) were harvested with TRIzol reagent (Life Technologies) and RNA was isolated according to the manufacturer's instructions. RNA samples were processed into cDNA libraries based on the CEL-seq2 technique as described previously^{73,74}. Illumina sequencing libraries were prepared with the TruSeq small RNA primers (Illumina) and were sequenced paired-end at 75-bp read length on an Illumina NextSeq. Tissue samples and tubuloids were processed and sequenced in parallel.

RNA-seq data analysis. Paired-end reads from Illumina sequencing were aligned to the human transcriptome with BWA⁷⁵. Reads were normalized and differential gene expression analysis performed using the DESeq2 package⁷⁶. Per gene, Z-scores of normalized expression were calculated and the results were depicted on a heatmap. Analyses, quantification and data visualization were run on Rstudio.

Bulk sequencing data can be found in the Supplementary Information and have been deposited at the GEO under accession code [GSE107795](#).

BK virus experiments. BK virus infection. Tubuloids were harvested, Matrigel was removed with cold ADMEM/F12, tubuloids were centrifuged, supernatant was taken off and tubuloids were subsequently incubated in ADMEM/F12 with crude BK virus (in Fig. 3a–e, g, h a clinical isolate genotype BK1b-1, isolated from urine of an immunocompromised patient, was first propagated in MRC5 cells; in Fig. 3f infected urine was used directly) for 2 h at 37°C, with regular mixing. The genome equivalent used for the infections was 2.5×10^5 IU ml⁻¹ (measured directly after incubation) and for the infections established with urine it was 6.3×10^3 IU ml⁻¹. After incubation, tubuloids were centrifuged and after a wash step with ADMEM/F12, tubuloids were plated out in Matrigel. Samples were harvested either directly after incubation or after different periods in culture (1, 2, 5, 10 or 30 d after incubation; with the 30 day time point for sequencing of BK virus) in 500 μ l of ADMEM/F12 and stored at -20°C until analysis.

Supernatant infection. 400 μ l of supernatant of a well (with 40 μ l of Matrigel) that was infected 30 d before, was harvested and diluted 1:15 in ADMEM/F12. Subsequently, it was filtered with a Millex-GS 0.22 μ m sterile filter unit (Merck Millipore) to remove cells, and this was used to infect tubuloids as described above. The genome equivalent used for the infections was 9.0×10^4 IU ml⁻¹ (measured directly after incubation). Samples were harvested either directly after incubation or after 10 d in culture in 500 μ l of ADMEM/F12 and stored at -20°C until analysis.

CDV inhibition experiment. Tubuloids were infected as described under BK virus infection. Tubuloids were cultured in tubuloid culture medium, supplemented with a range of concentrations of (0, 10, 20, 40, 80, 160, 320 μ g ml⁻¹) of CDV (Selleckchem). A non-infected control was exposed to 80 μ g ml⁻¹ CDV. Tubuloids were harvested after 7 d of culture and, during this period, culture media were refreshed twice. Samples were harvested in 500 μ l of ADMEM/F12 and stored at -20°C until analysis.

BK virus DNA extraction and real-time TaqMan PCR. Viral DNA was isolated using a MagNaPure 96 automated extraction system (Roche). Phocine herpes virus was added to the material before DNA extraction as an internal control. Samples were assayed in a 25 μ l reaction mixture containing 10 μ l of isolate, Taqman universal PCR mastermix (Applied Biosystems, ABI), primers (300 nM diagnostic primers; BK-forward: TGCTGATATTTGGGCTGTTTACTA; BK-reverse: CTCAGGCGRATCTTAAAATATCTTG) and fluorogenic probe (200 nM diagnostic probe; probe A: CAGCTCTGGAAACAACAGTGGAGAGGC; probe G: CAGCTC TGGGACACAACAGTGGAGAGGC) labeled with 5' reporter dye (FAM) and 3' quencher dye (TAMRA).

The amplification and detection were performed with an ABI 7500 system for 2 min at 50°C, 10 min at 95°C and 45 cycles of 15 s at 95°C and 1 min at 60°C. Samples were controlled for the presence of possible inhibitors of the amplification reaction by the indicated internal control, for which the signals had to be within the reference range.

Transmission electron microscopy. Tubuloids were infected as described under BK virus infection and a negative control was included. Tubuloids (80 μ l of Matrigel) were harvested after 10 d of culture. Matrigel was removed with recovery solution (Corning). Recovery solution was removed and 200 μ l of Karnovsky reagent was added. Samples were processed for transmission electron microscopy as described previously⁷⁹. Imaging was done with a FEI Tecnai T12 (80 kV).

Sequencing of BK virus DNA. The whole genome sequence of BK virus was obtained with the use of a modified sequence method⁸⁰. BK virus PCR fragments were obtained by fractional amplification of MagNAPure 96 total DNA isolates using the Superscript III one-step RT-PCR System (Thermo Fisher; the cDNA step was omitted (15–30 min at 45–60°C) and the process was started directly with heat inactivation of Superscript III RT (2 min at 94°C)) with a Platinum Taq High-Fidelity Kit (Invitrogen) and a 9800 Fast thermal cycler (ABI) according to the manufacturer's protocol. PCR products were applied to a 1% agarose gel and purified from the gel with the use of a GeneJet PCR purification kit (Thermo Scientific). Isolated fragments were used for WGS. Sequencing was performed by MacroGen Europe (Amsterdam, the Netherlands). The resulting sequence information was assembled into BK virus whole genome sequences through alignment with the reference BK virus genome GenBank accession code [V01108](#). Sequencing primers can be found in Supplementary Table 1.

SV40 stain. See Histology and immunohistochemistry.

Negative controls. Importantly, the negative controls that were included in the BK virus experiments showed no evidence for infection with BK virus or other polyomavirus that can be detected by antibodies to SV40. We performed PCRs on tubuloids before and at multiple time points after incubation with BK virus to assess BK virus replication. All samples consistently tested negative before inoculation with BK virus. The sequence of BK virus, harvested from tubuloid culture, was identical with the sequence of the strain added to the tubuloid culture, which indicates that the added strain had replicated and it was not some other, potentially latent BK virus strain.

Genotyping. DNA from tubuloids and tissue was isolated with a gDNA ReliaPrep Kit (Promega) according to the manufacturer's instructions. Primers for PCR amplification of *WT1* with Phusion High-Fidelity Polymerase (Thermo Scientific), were, for exon 7 (ref. ⁸¹), fw (5'-ACCTACGTGAATGTTCCATG-3') and rv (5'-GTTTGCCCAAGACTGGA-3') and for exon 10, fw (5'-GTGAAAAGCCCTTCAGCTGTC-3') and rv (5'-AAGGGTCAGGGGACATGAT-3'). Products were cloned into a CloneJET vector (Thermo Scientific) and sequenced using a T7 sequencing primer.

Low-coverage WGS for copy number profiling. Genome wide copy number alterations were established using low-coverage WGS. Shotgun libraries were prepared using the TruSeq Nano DNA Library Prep Kit (Illumina) according to the manufacturer's recommendations.

Briefly, 50–180 ng of input DNA (obtained with a Promega gDNA ReliaPrep Kit) from the primary tissues and the tubuloids were fragmented to 300 bp in 130 μ l using the Covaris System (Covaris). After concentrating the volume to 50 μ l, end repair, A-tailing and adapter ligation were performed following the manufacturer's instructions. For selective amplification of the library fragments that have adapter molecules on both ends we used 12 PCR cycles. Libraries were quality checked on an Agilent Bioanalyzer using a DNA 7500 Chip (Agilent Technologies) and quantified using qPCR with a commercially available PhiX library (Illumina) as a standard. Libraries were pooled equimolarly and sequenced on an Illumina NextSeq in a 150-bp single read run. Copy number analysis was performed as previously described⁸². Briefly, low-coverage WGS reads were mapped to the pseudo-autosomal-region masked genome and reads in different windows (~55 kb) were counted and normalized by the total number of reads. We further normalized read counts according to the GC content using LOWESS statistics. To avoid position effects we normalized the sequencing data with GC-normalized read counts of control samples. Subsequently, we generated segments of similar copy number values by applying circular binary segmentation and gain and loss analysis of DNA.

Real-time qPCR. Tubuloids were lysed and homogenized and total RNA was extracted with an RNEasy Mini Kit (Qiagen), according to the supplier's protocol. cDNA was synthesized from the RNA template using Moloney murine leukemia virus reverse transcriptase, RNase H Minus, Point Mutant (Promega) as per manufacturer's instructions. The resulting cDNA was diluted and this was used to determine expression levels. The reference genes used were *GAPDH* or *RPLP0*. Expression levels of the following genes were measured: *SIX2* (ref. ⁸³), *ANPEP*, *ABCC4*, *SLC4A4*, *SLC12A1*, *CLDN10*, *SLC12A3*, *SLC41A3*, *PCBD1*, *AQP3* and *NR3C2*. Primer sequences, all used at 60°C, except *SIX2* (which was used at 61°C), can be found in Supplementary Table 2.

The iQ SYBR Green Supermix (Bio-Rad) was used to multiply and measure the cDNA with a CFX96 or CFX384 Touch Real-Time PCR Detection System (Bio-Rad). Samples were run in triplicate in 20 μ l reactions (Fig. 4g) on a 96-well plate or

in duplicate in 12.5 µl reactions (Supplementary Fig. 10) on a 384-well plate in the following PCR program: 95 °C for 3 min, followed by 39 cycles of 10 s at 95 °C, 30 s at the indicated annealing temperature and 30 s at 72 °C, followed by a melt of the product from 65 °C to 95 °C.

mRNA expression of *SIX2* was normalized to GAPDH mRNA and expressed as fold change to the matched normal tubuloid line with the $\Delta\Delta\text{CT}$ method (Fig. 4g). In normal samples, no *SIX2* expression was detected after 39 cycles and therefore, for calculation of the fold change, the value 40 was used. This most likely leads to an underestimation of the *SIX2* upregulation in the tumor-derived tumoroids. qPCR products were loaded on an agarose gel to confirm a single product of the expected size (152 bp) and to show the difference between healthy tissue-derived tubuloids and tumor-derived tumoroids.

mRNA expression of *ANPEP*, *ABCC4*, *SLC4A4*, *SLC12A1*, *CLDN10*, *SLC12A3*, *SLC41A3*, *PCBD1*, *AQP3* and *NR3C2* was normalized to *RPLP0* mRNA and expressed as the fold change to human colon organoids cultured in expansion conditions (established and cultured as previously described⁷) with the $\Delta\Delta\text{CT}$ method (Supplementary Fig. 10).

P-gp transporter assay. Tubuloids were mechanically disrupted and seeded in BME on either glass bottom plates (for confocal imaging) or an opaque 96-well plate (for quantification in a fluorescence plate reader). Medium with or without P-gp-inhibitor PSC-833 (Tocris biosciences) at 5 µM was added. The next day, calcein-AM (1 µM, R&D Systems) was added with or without 5 µM PSC-833. After 1 h of incubation at 37 °C, the medium was removed and the cells were washed twice with 200 µl of ice-cold Hank's Balanced Salt Solution (HBSS). Then, cells were either fixed in 2% (w/v) paraformaldehyde (for confocal analysis) or cells were lysed by addition of 100 µl of 1% (v/v) Triton X-100 (fluorescent plate reader). Samples were used directly for analysis with a confocal microscope (SP5 or SP8, Leica) or a fluorescence plate reader (Ascent Fluoroskan FL microplate reader) with an excitation wavelength λ of 488 nm and an emission λ of 518 nm.

Forskolin (FSK) swelling assay and intestinal organoid culture. The FSK-induced swelling assay and intestinal organoid culture were carried out as described previously⁵, with the difference that swelling was monitored for 3 h after addition of FSK (8 nM and 5 µM), in both intestinal organoids and urine-derived tubuloids.

Organ-on-a-chip-plates—OrganoPlates. Cell culture. In each of the 40 chips in the three-lane 400 µm OrganoPlate microfluidic system (Mimetas, 4003400B), 2 µl of ECM gel composed of 4 mg ml⁻¹ Collagen I (AMSbio Cultrex 3D Collagen I Rat Tail, 5 mg ml⁻¹), 100 mM HEPES (Life Technologies) and 3.7 mg ml⁻¹ NaHCO₃ (Sigma) was dispensed in the gel inlet, incubated for 30 min at 37 °C and covered with 30 µl HBSS (Sigma). The next day, tubuloids were trypsinized, made into a single-cell suspension and applied to the OrganoPlate by seeding 2 µl of 10 × 10⁶ cells per ml in the inlet of the top medium channel. Next, 50 µl of human tubuloid culture medium was added to the same inlet and the plate was placed on the side in an incubator for 5 h to allow the cells to attach to the ECM. Afterwards, an additional 50 µl of culture media was added to each of the remaining in- and outlets of the top and bottom medium channels. Subsequently, the OrganoPlate was placed horizontally in the incubator (37 °C, 5% CO₂) on an interval rocker (every 8 min switching between +7° and -7° inclination) allowing bi-directional flow with a mean flow rate of 2.02 µl min⁻¹ and a mean shear of 0.13 Pa. The medium (50 µl each on the in- and outlets) was refreshed every 2 to 3 d. After 7 d, cells were either formaldehyde fixed for immunofluorescent staining or used for barrier integrity or transport assays.

Immunofluorescence in OrganoPlates. Kidney tubuloid-derived tubules cultured in the OrganoPlate were fixed with 50 µl of 3.7% formaldehyde (Sigma) in HBSS for 15 min, washed twice with HBSS and permeabilized with 0.3% Triton X-100 (Sigma) in HBSS for 10 min. Next, cells were washed with 4% FCS (Sigma) in HBSS and incubated with blocking solution (2% FCS, 2% BSA (Sigma), 0.1% Tween20 (Sigma) in HBSS) for 30 min. Afterwards, cells were incubated with primary antibodies for 1 h at room temperature, washed twice, incubated with secondary antibodies for 30 min at room temperature and washed twice with 4% FCS in HBSS. The following antibodies were used: mouse anti-Ezrin (1:125, catalog. no. 610602, BD Transduction), rabbit anti-ZO1 (5 µg ml⁻¹, catalog. no. 617300, Life Technologies), rabbit anti-CDH1 (1:200, catalog. no. 31955, Cell Signaling Technology), rabbit anti-Na/K-ATPase (1:400, catalog. no. ab76020, Abcam), mouse anti-acetylated tubulin (1:2,000, catalog. no. T6793, Sigma), mouse isotype (Life Technologies), rabbit isotype (Life Technologies), goat anti-mouse Alexa Fluor 647 (Life Technologies, 1:250) and goat anti-rabbit Alexa Fluor 488 (Life Technologies, 1:250). Finally, the nuclei were stained with Hoechst 33342 (Life Technologies) and cells were stored in HBSS. The kidney tubuloid-derived tubules were imaged with ImageXpress Micro XLS-C High Content Imaging System (Molecular Devices).

Barrier integrity assay. Medium in the apical perfusion channel was replaced by medium containing 0.5 mg ml⁻¹ FITC-dextran (20 kDa, Sigma) and 0.5 mg ml⁻¹ TRITC-dextran (155 kDa). Leakage of the fluorescent dye from the lumen of the

renal tubular structure into the ECM compartment was imaged every 5 min for at least 30 min on an ImageXpress XLS Micro (Molecular Devices) or Leica SP5.

P-gp transport assay. Cells were incubated with calcein-AM (Life Tech, 1 µM) at the apical side of the tube in the presence or absence of PSC-833 (Sigma) at 5 µM in OptiHBSS (33% Opti-MEM (Gibco)), 66% HBSS (Sigma) for 1 h in the incubator (37 °C, 5% CO₂) on an interval rocker (8 min, 7°). After incubation, cells were washed once with OptiHBSS, nuclei were stained with Hoechst 33342 and the tubes were imaged with ImageXpress Micro XLS-C High Content Imaging System (Molecular Devices). The intracellular fluorescent values were corrected for total cell numbers of each microfluidic chip, for background values, and were normalized to the calcein-AM only condition.

Trans-epithelial transport assay. Medium in the apical channel was replaced with medium containing 5 µM PSC-833 or 0.2% DMSO. Medium in the basal channel was replaced with medium containing 10 µM rhodamine 123 (Sigma) and 5 µM PSC-833 or 0.2% DMSO, respectively. To determine the concentration of rhodamine 123, a concentration curve was added to extra chips. Tubules were incubated for 5 h on the rocker (8 min, 7°) in the incubator (37 °C, 5% CO₂). After 3 and 5 h, the rhodamine 123 concentration was measured by imaging the top inlets with the FITC filter on the ImageXpress Micro XLS-C High Content Imaging System (Molecular Devices). The apparent permeability (P_{app} , in cm s⁻¹) was calculated by using the following formula:

$$P_{\text{app}} = \frac{\Delta C_{\text{receiver}} \times V_{\text{receiver}}}{\Delta t \times A \times C_{\text{donor}}}$$

where C_{receiver} is the measured intensity difference in the top wells over time, V_{receiver} is the receiving volume in the reservoirs of the top inlets, t is the time difference, A is the surface of the ECM interface with the medium channel and C_{donor} is the donor concentration of 10 µM rhodamine 123.

Statistics. In the BK virus experiments (Fig. 3e,g,h) and the forskolin swelling assays (Fig. 5d), the means of the three independent experiments were compared in a non-paired two-tailed t -test, or a one-way ANOVA was performed, combined with Tukey post-hoc tests (Fig. 3h). The forskolin swelling assays were performed in duplicate and for the virus experiments PCRs were performed in duplicate. For the transporter assays, where multiple independent measurements were taken on distinct 'tubuloids-on-a-chip' and where a relative difference between start and end is considered, values were normalized to negative controls (Fig. 6i; $n \geq 3$ for each of the independent experiments; Supplementary Fig. 9, $n \geq 5$ for each of the 3 independent experiments). The normalized measurements were then grouped to calculate the significance with a non-paired two-tailed t -test. For Fig. 6j (two independent experiments with $n = 20$ and $n = 14$), the values of the independent experiments were grouped to calculate the significance with a non-paired two-tailed t -test.

For the single-cell RNA-seq, differential expression was performed using the Wilcoxon test with 1.8-fold expression cut-off and 5% Bonferroni multiple-testing corrected statistical significance cut-off. For bulk RNA-seq, reads were normalized and differential gene expression analysis performed using the DESeq2 package⁷⁸. Per gene, Z -scores of normalized expression were calculated and the results were depicted on a heatmap.

A $P < 0.05$ was considered statistically significant.

Reporting Summary. Further information on research design is available in the Nature Research Reporting Summary linked to this article.

Data availability

The data that support the findings of this study are available from the corresponding author upon reasonable request. WGS data have been deposited at the EGA, which is hosted by the EBI, under accession code [EGAS00001002729](https://ega-archive.org/studies/EGAS00001002729). Single-cell and bulk sequencing data can be found in the Supplementary Information and have been deposited at GEO under accession code [GSE107795](https://www.ncbi.nlm.nih.gov/geo/query/acc.cgi?acc=GSE107795).

References

- Kim, K.-A. et al. Mitogenic influence of human R-Spondin1 on the intestinal epithelium. *Science* **309**, 1256–1259 (2005).
- Huch, M. et al. In vitro expansion of single Lgr5+ liver stem cells induced by Wnt-driven regeneration. *Nature* **494**, 247–250 (2013).
- Drost, J. et al. Use of CRISPR-modified human stem cell organoids to study the origin of mutational signatures in cancer. *Science* **358**, 234–238 (2017).
- Barker, N. et al. Lgr5(+ve) stem cells drive self-renewal in the stomach and build long-lived gastric units in vitro. *Cell Stem Cell* **6**, 25–36 (2010).
- Muraro, M. J. et al. A single-cell transcriptome atlas of the human pancreas. *Cell Syst* **3**, 385–394 (2016).
- Hashimshony, T. et al. CEL-Seq2: sensitive highly-multiplexed single-cell RNA-Seq. *Genome Biol.* **17**, 77 (2016).
- Li, H. & Durbin, R. Fast and accurate short read alignment with Burrows-Wheeler transform. *Bioinformatics* **25**, 1754–1760 (2009).

76. Satija, R., Farrell, J. A., Gennert, D., Schier, A. F. & Regev, A. Spatial reconstruction of single-cell gene expression data. *Nat. Biotechnol.* **33**, 495–502 (2015).
77. Tirosh, I. et al. Dissecting the multicellular ecosystem of metastatic melanoma by single-cell RNA-seq. *Science* **352**, 189–196 (2016).
78. Love, M. I., Huber, W. & Anders, S. Moderated estimation of fold change and dispersion for RNA-seq data with DESeq2. *Genome Biol.* **15**, 550 (2014).
79. Galmes, R. et al. Vps33B is required for delivery of endocytosed cargo to lysosomes. *Traffic* **16**, 1288–1305 (2015).
80. Tan, L. et al. Genetic variability among complete human respiratory syncytial virus subgroup A genomes: bridging molecular evolutionary dynamics and epidemiology. *PLoS ONE* **7**, e51439 (2012).
81. Coppes, M. J., Liefers, G. J., Paul, P., Yeger, H. & Williams, B. R. Homozygous somatic Wt1 point mutations in sporadic unilateral Wilms tumor. *Proc. Natl Acad. Sci. USA* **90**, 1416–1419 (1993).
82. Heitzer, E. et al. Tumor-associated copy number changes in the circulation of patients with prostate cancer identified through whole-genome sequencing. *Genome Med.* **5**, 30 (2013).

Reporting Summary

Nature Research wishes to improve the reproducibility of the work that we publish. This form provides structure for consistency and transparency in reporting. For further information on Nature Research policies, see [Authors & Referees](#) and the [Editorial Policy Checklist](#).

Statistical parameters

When statistical analyses are reported, confirm that the following items are present in the relevant location (e.g. figure legend, table legend, main text, or Methods section).

n/a | Confirmed

- The exact sample size (n) for each experimental group/condition, given as a discrete number and unit of measurement
- An indication of whether measurements were taken from distinct samples or whether the same sample was measured repeatedly
- The statistical test(s) used AND whether they are one- or two-sided
Only common tests should be described solely by name; describe more complex techniques in the Methods section.
- A description of all covariates tested
- A description of any assumptions or corrections, such as tests of normality and adjustment for multiple comparisons
- A full description of the statistics including central tendency (e.g. means) or other basic estimates (e.g. regression coefficient) AND variation (e.g. standard deviation) or associated estimates of uncertainty (e.g. confidence intervals)
- For null hypothesis testing, the test statistic (e.g. F , t , r) with confidence intervals, effect sizes, degrees of freedom and P value noted
Give P values as exact values whenever suitable.
- For Bayesian analysis, information on the choice of priors and Markov chain Monte Carlo settings
- For hierarchical and complex designs, identification of the appropriate level for tests and full reporting of outcomes
- Estimates of effect sizes (e.g. Cohen's d , Pearson's r), indicating how they were calculated
- Clearly defined error bars
State explicitly what error bars represent (e.g. SD, SE, CI)

Our web collection on [statistics for biologists](#) may be useful.

Software and code

Policy information about [availability of computer code](#)

Data collection

No software was used for data collection.

Data analysis

Microsoft Excel (different versions, including 2007, 2010 for Windows and for Mac), GraphPad Prism 7, Imaris, LAS X, Leica AF Lite, GATK HaplotypeCaller v3.4–46, BWA and DESeq2. No code was used that has not been published before.

For manuscripts utilizing custom algorithms or software that are central to the research but not yet described in published literature, software must be made available to editors/reviewers upon request. We strongly encourage code deposition in a community repository (e.g. GitHub). See the Nature Research [guidelines for submitting code & software](#) for further information.

Data

Policy information about [availability of data](#)

All manuscripts must include a [data availability statement](#). This statement should provide the following information, where applicable:

- Accession codes, unique identifiers, or web links for publicly available datasets
- A list of figures that have associated raw data
- A description of any restrictions on data availability

The data that support the findings of this study are available from the corresponding author upon reasonable request. Sequencing data has been deposited in publicly available depositories with accession codes GSE107795 and EGAS00001002729.

Field-specific reporting

Please select the best fit for your research. If you are not sure, read the appropriate sections before making your selection.

Life sciences Behavioural & social sciences Ecological, evolutionary & environmental sciences

For a reference copy of the document with all sections, see [nature.com/authors/policies/ReportingSummary-flat.pdf](https://www.nature.com/authors/policies/ReportingSummary-flat.pdf)

Life sciences study design

All studies must disclose on these points even when the disclosure is negative.

Sample size	No sample-size calculation was performed. When quantitative data were obtained, sample sizes were based on previously published studies on this type of measurements and assays (e.g. Dekkers et al. Nature Medicine, 2013 for forskolin swelling assays and Jansen et al. Exp. Cell. Res., 2014). In most experiments, qualitative data were obtained (e.g. microscopy images of tumor versus normal) rather than quantitative.
Data exclusions	No data were excluded.
Replication	Attempts at replication were successful in multiple tubuloid lines grown under the same conditions.
Randomization	Samples were allocated randomly to different experimental groups.
Blinding	Blinding was not possible during data collection (e.g. tumor tissue is clearly distinct from healthy kidney tissue). In the virus experiments, analysis was carried out by a different person than the one responsible for data collection. In the forskolin swelling assays and single cell RNA sequencing experiments, analysis was carried out with an algorithm, excluding bias.

Reporting for specific materials, systems and methods

Materials & experimental systems

n/a	Involvement in the study
<input checked="" type="checkbox"/>	<input type="checkbox"/> Unique biological materials
<input type="checkbox"/>	<input checked="" type="checkbox"/> Antibodies
<input type="checkbox"/>	<input checked="" type="checkbox"/> Eukaryotic cell lines
<input checked="" type="checkbox"/>	<input type="checkbox"/> Palaeontology
<input type="checkbox"/>	<input checked="" type="checkbox"/> Animals and other organisms
<input type="checkbox"/>	<input checked="" type="checkbox"/> Human research participants

Methods

n/a	Involvement in the study
<input checked="" type="checkbox"/>	<input type="checkbox"/> ChIP-seq
<input checked="" type="checkbox"/>	<input type="checkbox"/> Flow cytometry
<input checked="" type="checkbox"/>	<input type="checkbox"/> MRI-based neuroimaging

Antibodies

Antibodies used

All antibodies were used against human tissue.
 rabbit anti-Pax8 (1:500, 10336-1-AP, Proteintech). Manufacturer's website: validated for IHC on human tissue.
 mouse anti-P63 (1:50, M7317, Dako). Manufacturer's website: validated for IHC on human tissue.
 mouse anti-SV-40 (1:100, bPAb416, Merck Millipore): Manufacturer's website: validated for IHC for detection of large T antigen.
 mouse anti-Ezrin (1:125, #610602 (clone 18), BD Transduction). Manufacturer's website: validated for IF on human tissue during development.
 rabbit anti-AQP-3 (1:100, 125219, Abcam). Manufacturer's website: validated for IF on human tissue.
 rabbit anti-AE1 / SLC4A1 (1:100, AE11-A, Alpha Diagnostics International). Manufacturer's website / datasheet: validated for IHC

on rat tissue. Epitope is 70% conserved in humans (in both erythrocyte and kidney) and others have used the antibody on western blot on human material (Rentsch et al 2006, J. Appl. Phys.)

goat anti-calbindin D28K (1:200, N-18, Santa Cruz). Manufacturer's website: validated for IF/IHC on human tissue.

Rabbit anti-Na⁺/K⁺ ATPase (1:400, #ab76020, Abcam). Manufacturer's website: validated for IF on human tissue.

Rabbit anti-NKCC2 (1:200) was provided by Prof. Hoenderop (Nijmegen, the Netherlands).

goat anti-GATA3 (1:300, AF2605, R&D Systems). Manufacturer's website: validated for IF on human tissue.

mouse E-Cadherin (1:300, 610182, BD Biosciences). Manufacturer's website: validated for IF on human tissue.

rabbit anti-Claudin-3 (1:200, AB15102, Abcam). Manufacturer's website: validated for IF on human tissue.

Rabbit anti-CDH1 (1:200, #31955, Cell Signaling Technology). Manufacturer's website: validated for IF on human tissue.

mouse anti-Integrin alpha-6 (1:200, AB20142, Abcam). Manufacturer's website: validated for IF on human tissue.

Rabbit anti-Na⁺/K⁺-ATPase (1:400, #ab76020, Abcam). Manufacturer's website: validated for IF on human tissue.

mouse anti-Villin (1: 200, SC-58897, Santa Cruz). Manufacturer's website: validated for IF on human tissue.

rabbit anti-ZO1 (1: 100, 402200, Thermo Fisher Scientific). Manufacturer's website: validated for IF on human tissue.

Rabbit anti-ZO-1 (5µg/ml, #617300, Life tech). Manufacturer's website: validated for IF on human tissue.

mouse anti-VP1 (1:2000, clone 3B2 SAB1412996, Sigma). Manufacturer's website: validated for detection of BK virus protein VP1 with IHC.

mouse anti-Acetylated Tubulin (1: 2000, SC-23950, Santa Cruz). Manufacturer's website: validated for IF on human tissue.

rabbit anti-cytokeratin (1: 20, Z0622, Dako). Manufacturer's website: validated for IF on human tissue.

Six2 (1:300, 11562-1-AP, Proteintech). Manufacturer's website: validated for IF on human tissue.

Goat-anti-Rabbit Powervision-Horse Radish Peroxidase (1:500, Dako). Manufacturer's website: validated for detection of rabbit IgG.

568 donkey anti-rabbit immunoglobulin G (IgG), Alexa Fluor 568 donkey anti-goat IgG, 488 donkey anti-rabbit IgG, 555 Donkey anti-mouse IgG (1:500, Thermo Scientific): Manufacturer's website: validated for detection of IgGs of the indicated species.

Validation

Validation statements are included in the 'Antibodies used' statement above.

Eukaryotic cell lines

Policy information about [cell lines](#)

Cell line source(s)

MRC5 cells

Authentication

Non authenticated, because it is not relevant, as the cell line was only used to produce BK virus

Mycoplasma contamination

Negative

Commonly misidentified lines
(See [ICLAC](#) register)

-

Animals and other organisms

Policy information about [studies involving animals](#); [ARRIVE guidelines](#) recommended for reporting animal research

Laboratory animals

We used the kidneys from adult, male and female, C57BL/6 mice for organoid culture.

Wild animals

Study did not involve wild animals.

Field-collected samples

Study did not involve field-collected samples.

Human research participants

Policy information about [studies involving human research participants](#)

Population characteristics

Both adult and pediatric, male and female human kidney tissue was included.

Recruitment

Anonymized kidney tissue became available after nephrectomy: this was left-over material that was not required for diagnosis and no informed consent was required (i.e. no recruitment), on the condition that cultured material was destroyed after one year. For the organoid line that was used for the WGS analysis, informed consent was obtained using the Hubrecht Organoid Technology (HUB) approved protocol. In two instances, we included pediatric Wilms tumor tissue for our study for which informed consent was obtained by the treating physician. Selection of these patients was random, to prevent bias.